Inorg. Chem. **2004**, *43*, 1574–1586

New Poly-Iron(II) Complexes of N_4O Dinucleating Schiff Bases and Pseudohalides: Syntheses, Structures, and Magnetic and Mössbauer Properties

Athanassios K. Boudalis,[†] Juan-Modesto Clemente-Juan,[‡] Françoise Dahan, and Jean-Pierre Tuchagues*

Laboratoire de Chimie de Coordination, UPR CNRS 8241, 205, Route de Narbonne, 31077 Toulouse, France

Received October 15, 2003

Six dinuclear ferrous complexes including $[Fe_2(acpypentO)(O_2CMe)(NCS)_2]$ (**1**), $[Fe_2(acpypentO)(O_2CMe)(NCSe)_2]$ (**2**), $[Fe_2(acpypentO)(NCO)_3]$ (**3**), $([Fe_2(acpybutO)(O_2CMe)(NCS)_2]$ (**5**), $[Fe_2(acpybutO)(O_2CMe)(NCO)_2]$ (**6**), and $[Fe_2(acpybutO)(O_2CMe)(N_3)_2]$ (**7**), one tetranuclear (bis-dinuclear) ferrous compound, $[Fe_4(acpypentO)_2(N_3)_6]$ (**4**), and one mononuclear ferrous compound, $[Fe(acpybutOH)(NCS)_2]$ (**8**), have been prepared, and their structures and magnetic and Mössbauer properties have been studied (acpybutOH = 1,4-bis{[2-pyridyl(1-ethyl]imino)}butane-2-ol and acpypentOH = 1,5-bis{[2-pyridyl(1-ethyl]imino)}pentane-3-ol). The X-ray diffraction analyses yielded the following results: **1** ($C_{23}H_{26}Fe_2N_6O_3S_2$, monoclinic, $P2_1/n$, a = 8.0380(7) Å, b = 12.4495(8) Å, c = 27.358(2) Å, β = 92.180(10)°, V = 2735.7(4) Å^3, Z = 4) is a dinuclear species in which the unequivalent high-spin (HS) Fe^{II} sites are bridged by the alkoxo oxygen atom of the symmetrical acpypentO$^-$ Schiff base and one syn–syn acetato anion; **3** ($C_{22}H_{23}Fe_2N_7O_4$, triclinic, $P\bar{1}$, a = 8.4152(10) Å, b = 9.1350(10) Å, c = 17.666(2) Å, α = 97.486(14)°, β = 100.026(14)°, γ = 113.510(13)°, V = 1195.9(2) Å^3, Z = 2) is a dinuclear species in which the unequivalent HS Fe^{II} sites are bridged by the alkoxo oxygen atom of the symmetrical acpypentO$^-$ Schiff base and one end-on NCO anion; **4**-MeOH ($C_{39}H_{50}Fe_4N_{26}O_3$, triclinic, $P\bar{1}$, a = 9.1246(11) Å, b = 10.2466(11) Å, c = 14.928(2) Å, α = 91.529(15)°, β = 101.078(16)°, γ = 106.341(14)°, V = 1309.6(3) Å^3, Z = 1) is a bis-dinuclear species in which the unequivalent HS Fe^{II} sites are bridged by the alkoxo oxygen atom of the symmetrical acpypentO$^-$ Schiff base and one end-on N_3^- anion, and the symmetry related Fe^{II} sites are bridged by two end-on N_3^- anions; **8**-MeOH ($C_{21}H_{26}FeN_6O_2S_2$, triclinic, $P\bar{1}$, a = 8.7674(9) Å, b = 12.0938(13) Å, c = 12.2634(14) Å, α = 106.685(14)°, β = 93.689(14)°, γ = 108.508(13)°, V = 1163.7(2) Å^3, Z = 2) is a mononuclear species in which the octahedral low-spin (LS) Fe^{II} site is in an N_6 environment provided by the four N atoms of the protonated asymmetrical acpybutOH Schiff base and two thiocyanato anions. The Mössbauer spectra of all dinuclear species (**1**–**3** and **5**–**7**), and of the bis-dinuclear compound **4**, evidence two distinct HS Fe^{II} sites while the Mössbauer spectra of the mononuclear compound **8** evidence a LS Fe^{II} site over the 80–300 K temperature range. The temperature dependence of the magnetic susceptibility was fitted with J = –13.7 cm^{-1}, D = –1.8 cm^{-1}, and g = 2.096 for **1**; J = 3.0 cm^{-1}, D_1 = 1.6 cm^{-1}, E_1 = –0.35 cm^{-1} (λ_1 = 0.22), D_2 = – 12.2 cm^{-1}, E_2 = 1.1 cm^{-1} (λ_2 = 0.09), and g = 2.136 for **3**; and J_1 = – 0.09 cm^{-1}, J_2 = 15.9 cm^{-1}, D_1 = 5.7 cm^{-1}, D_2 = 12.1 cm^{-1}, and g = 1.915 for **4**. The nature of the ground state in **3** and **4** was confirmed by simulation of the magnetization curves at 2 and 5 K. The intradinuclear interaction through the central O_{alkoxo} of the acpypentO$^-$ ligand and one pseudohalide bridges is ferromagnetic in **3** (end-on cyanato) while it is very weakly antiferromagnetic in **4** (end-on azido). The interdinuclear interaction through two end-on azido bridges (**4**) is ferromagnetic as expected. In agreement with the symmetry of the two iron sites of complexes **3** and **4**, the fits show that D_2 (tetragonal pyramid) is larger than D_1 (distorted trigonal bipyramid (**3**) or distorted octahedron (**4**)).

Introduction

Exploring the possibilities of extending poly-iron chemistry in a controlled fashion is of the utmost importance to the promising field of molecular-based magnetic materials.[1] To this aim, we have recently suggested the use of dinucleating ligands selected for generating coordinatively deficient ferrous species prone to bind pseudohalide anions as bridging ligands concurrently to oxygen bridges, and we have described the syntheses, structure, and magnetic properties of the first examples of such poly-iron compounds.[2] The dinucleating pentadentate ligand with a N_4O donor set

* To whom correspondence should be addressed. E-mail: tuchague@lcc-toulouse.fr.

[†] Present address: Department of Chemistry, University of Patras, 26504 Patras, Greece.

[‡] Present address: Instituto de Ciencia Molecular, Universidad de Valencia, c/ Doctor Moliner, 50, 46100 Burjassot, Spain.

10.1021/ic0351904 CCC: $27.50
Published on Web 01/30/2004

Scheme 1

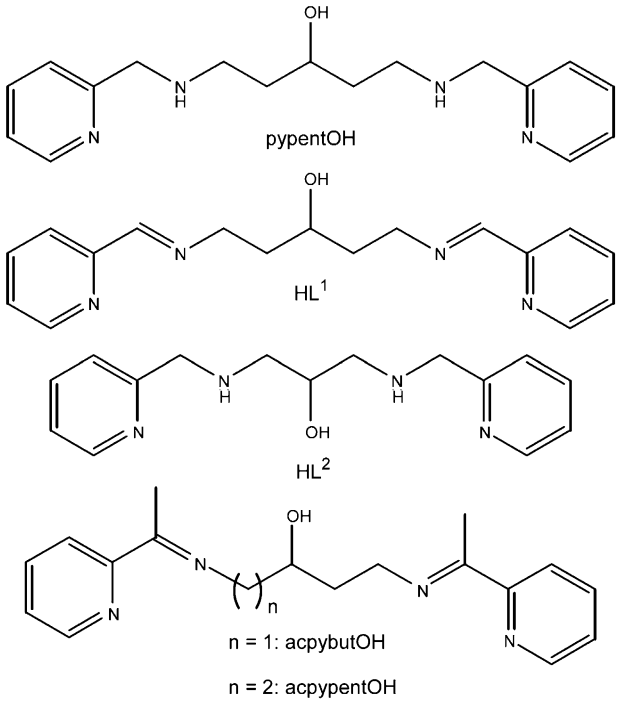

designed for this first exploration, 1,5-bis[(2-pyridylmethyl)-amino]pentane-3-ol (pypentOH, Scheme 1), was produced through reduction of the imine functions of the corresponding Schiff base, 1,5-bis[(2-pyridylmethyl)imino]pentane-3-ol (HL[1], Scheme 1), which itself results from the bis-condensation of 1,5-diaminopentan-3-ol with 2-pyridine carboxaldehyde. Copper(II) dinuclear complexes of HL[1], and of its reduced pypentOH form, have been reported, where the Cu^{II} ions are bridged by the alkoxo oxygen of the pentadentate ligand and one hydroxo, chloro, bromo, acetato, or pyrazolato anion.[3] More recently, one tetranuclear nickel(II) complex of the pentadentate pypentOH ligand has been reported, where the Ni^{II} ions are bridged by the alkoxo oxygen of pypentOH, the alkoxo oxygen of the 2-pyridylmethanol ancillary ligand, two hydroxo, and two acetato anions.[4] Dinuclear copper-(II)[3b] and mono- and dinuclear manganese(II) complexes[5] of the related HL[2] ligand (Scheme 1), i.e., the reduced form of the Schiff base resulting from the bis-condensation of 1,3-diaminopropan-2-ol with 2-pyridine carboxaldehyde, have also been reported, none of them including a pseudohalide bridge. While discrete pseudohalide-bridged complexes are common for transition metal ions such as copper(II),[6] nickel-(II),[7] cobalt(III),[8] manganese(II),[7] and iron(III),[9] they are scarce for iron(II).[2] On the other hand, a few examples of pseudohalide-bridged 1D to 3D chains have recently been reported where azido anions bridge iron(II) centers in either the μ-1,1 (end-on) mode,[10] or μ-1,3 (end-to-end) mode,[11] or in both modes.[11] In the present contribution, we consider the iron(II) chemistry of two novel Schiff bases in the presence of pseudohalide anions (NCS^-, $NCSe^-$, N_3^-). The pentadentate (N_4O) Schiff bases resulting from the bis-condensation of 1,4-diaminobutan-2-ol and 1,5-diaminopentan-3-ol with 2-acetylpyridine, 1,4-bis{[2-pyridyl(1-ethyl]-imino)}butane-2-ol, and 1,5-bis{[2-pyridyl(1-ethyl]imino)}-pentane-3-ol are abbreviated (acpybutOH) and (acpypentOH), respectively (Scheme 1).

Six dinuclear ferrous compounds including $[Fe_2(acpypentO)(O_2CMe)(NCS)_2]$ (**1**), $[Fe_2(acpypentO)(O_2CMe)(NCSe)_2]$ (**2**), $[Fe_2(acpypentO)(NCO)_3]$ (**3**), $([Fe_2(acpybutO)(O_2CMe)(NCS)_2]$ (**5**), $[Fe_2(acpybutO)(O_2CMe)(NCO)_2]$ (**6**), and $[Fe_2(acpybutO)(O_2CMe)(N_3)_2]$ (**7**), one tetranuclear (bis-dinuclear) ferrous compound, $[Fe_4(acpypentO)_2(N_3)_6]$ (**4**), and one mononuclear ferrous compound, [Fe(acpybutOH)$(NCS)_2$] (**8**), have been obtained, the preparation,

(1) (a) McCusker, J. K.; Christmas, C. A.; Hagen, P. M.; Chadha, R. K.; Harvey, D. F.; Hendrickson, D. N. *J. Am. Chem. Soc.* **1991**, *113*, 6114. (b) Taft, K. L.; Delfs, C. D.; Papaefthymiou, G. C.; Foner, S.; Gatteschi, D.; Lippard, S. J. *J. Am. Chem. Soc.* **1994**, *116*, 823. (c) Powell, A. K.; Heath, S. L.; Gatteschi, D.; Pardi, L.; Sessoli, R.; Spina, G.; Del Giallo, F.; Pieralli, F. *J. Am. Chem. Soc.* **1995**, *117*, 2491. (d) Benelli, C.; Parsons, S.; Solan, G. A.; Winpenny, R. E. P. *Angew. Chem.* **1996**, *35*, 1825. (e) Shweky, I.; Pence, L. E.; Papaefthymiou, G. C.; Sessoli, R.; Yun, J. W.; Bino, A.; Lippard, S. J. *J. Am. Chem. Soc.* **1997**, *119*, 1037. (f) Sangregorio, C.; Ohm, T.; Paulsen, C.; Sessoli, R.; Gatteschi, D. *Phys. Rev. Lett.* **1997**, *78*, 4645. (g) Barra, A. L.; Caneschi, A.; Cornia, A.; Fabrizi de Biani, F.; Gatteschi, D.; Sangregorio, C.; Sessoli, R.; Sorace, L. *J. Am. Chem. Soc.* **1999**, *121*, 5302. (h) Gatteschi, D.; Sessoli, R.; Cornia, A. *J. Chem. Soc., Chem. Commun.* **2000**, 725. (i) Goodwin, J. C.; Sessoli, R.; Gatteschi, D.; Wernsdorfer, W.; Powell, A. K.; Heath, S. L. *J. Chem. Soc., Dalton Trans.* **2000**, 1835. (j) Oshio, H.; Hoshino, N.; Ito, T. *J. Am. Chem. Soc.* **2000**, *122*, 12602. (k) Benelli, C.; Cano, J.; Journaux, Y.; Sessoli, R.; Solan, G. A.; Winpenny, R. E. P. *Inorg. Chem.* **2001**, *40*, 188. (l) Boudalis, A. K.; Lalioti, N.; Spyroulias, G. A.; Raptopoulou, C. P.; Terzis, A.; Tangoulis, V.; Perlepes, S. P. *J. Chem. Soc., Dalton Trans.* **2001**, 955. (m) Raptopoulou, C. P.; Tangoulis, V.; Devlin, E. *Angew. Chem., Int. Ed.* **2002**, *41*, 2386. (n) Jones, L. F.; Batsanov, A.; Brechin, E, K.; Collison, D.; Helliwell, M.; Mallah, T.; McInnes, E. J. L.; Piligkos, S. *Angew. Chem., Int. Ed.* **2002**, *41*, 4318. (o) Boudalis, A. K.; Lalioti, N.; Spyroulias, G. A.; Raptopoulou, C. P.; Terzis, A.; Bousseksou, A.; Tangoulis, V.; Tuchagues, J.-P.; Perlepes, S. P. *Inorg. Chem.* **2002**, *41*, 6474. (p) Sunatsuki, Y.; Ikuta, Y.; Matsumoto, N.; Ohta, H.; Kojima, M.; Iijima, S.; Hayami, S.; Maeda, Y.; Kaizaki, S.; Dahan, F.; Tuchagues, J.-P. *Angew. Chem., Int. Ed.* **2003**, *42*, 1614. (q) Boudalis, A. K.; Dahan, F.; Bousseksou, A.; Tuchagues, J.-P.; Perlepes, S. P. *Dalton Trans.* **2003**, 3411. (r) Low, D. M.; Jones, L. F.; Bell, A.; Brechin, E. K.; Mallah, T.; Rivière, E.; Teat, S. J.; McInnes, E. J. L. *Angew. Chem., Int. Ed.* **2003**, *42*, 3781. (s) Tolis, E. I.; Helliwell, M.; Langley, S.; Raftery, J.; Winpenny, R. E. P. *Angew. Chem., Int. Ed.* **2003**, *42*, 3804. (t) Ruben, B.; Breuning, E.; Lehn, J.-M.; Ksenofontov, V.; Renz, F.; Gütlich, P.; Vaughan, G. B. M. *Chem. Eur. J.* **2003**, *9*, 4422.

(2) Clemente-Juan, J. M.; Mackiewicz, C.; Verelst, M.; Dahan, F.; Bousseksou, A.; Sanakis, Y.; Tuchagues, J.-P. *Inorg. Chem.* **2002**, *41*, 1478.

(3) (a) Mazurek, W.; Berry, K. J.; Murray, K. S.; O'Connor, M. J.; Snow, M. R.; Wedd, A. G. *Inorg. Chem.* **1982**, *21*, 3071. (b) Mazurek, M.; Kennedy, B. J.; Murray, K. S.; O'Connor, M. J.; Rodgers, J. R.; Snow, M. R.; Wedd, A. G.; Zwack, P. R. *Inorg. Chem.* **1985**, *24*, 3258.

(4) Clemente-Juan, J. M.; Chansou, B.; Donnadieu, B.; Tuchagues, J.-P. *Inorg. Chem.* **2000**, *39*, 5515.

(5) (a) Mikuriya, M.; Hatano, Y.; Asato, E. *Bull. Chem. Soc. Jpn.* **1997**, *70*, 2495. (b) Mikuriya, M.; Fukumoto, H.; Kako, T. *Inorg. Chem. Commun.* **1998**, *1*, 225.

(6) See for example: (a) Maji, T. K.; Mukherjee, P. S.; Koner, S.; Mostafa, G.; Tuchagues, J.-P.; Chaudhuri, N. R. *Inorg. Chim. Acta*, **2001**, *314*, 111. (b) Koner, S.; Saha, S.; Okamoto, K.-I.; Tuchagues, J.-P. *Inorg. Chem.* **2003**, *42*, 4668 and references therein.

(7) See for example: Ribas, J.; Escuer, A.; Monfort, M.; Vicente, R.; Cortés, R.; Lezama, L.; Rojo, T. *Coord. Chem. Rev.* **1999**, *193*−*195*, 1027 and references therein.

(8) See for example: Drew, M. G. B.; Harding, C. J.; Nelson, J. *Inorg. Chim. Acta* **1996**, *246*, 73 and references therein.

(9) See for example: Reddy, K. R.; Rajasekharan, M. V.; Tuchagues, J.-P. *Inorg. Chem.* **1998**, *37*, 5978 and references therein.

(10) Hao, X.; Wei, Y.; Zhang, S. *J. Chem. Soc., Chem. Commun.* **2000**, 2271.

(11) Konar, S.; Zangrando, E.; Drew, M. G. B.; Mallah, T.; Ribas, J.; Chaudhuri, N. R. *Inorg. Chem.* **2003**, *42*, 5966.

characterization, X-ray crystal structure, and magnetic and Mössbauer study of which is presented in this report.

Experimental Section

Materials. All chemicals, unless otherwise stated, were commercially available and were used as received. Iron(II) acetate dihydrate was synthesized as previously described.[12] Solvents were analytically pure and were deoxygenated prior to use.

Syntheses. *Caution: Although no such behavior was observed during the present work, azido salts are potentially explosive and should be handled with care.*

Ligands. 1,5-Bis{[2-pyridyl(1-ethyl]imino)}pentane-3-ol (acpypentOH) and 1,4-Bis{[2-pyridyl(1-ethyl]imino)}butane-2-ol (acpybutOH). 1,5-Diaminopentan-3-ol dihydrochloride,[13] or 1,4-diaminobutan-2-ol dihydrochloride,[14] synthesized according to literature procedures, was deprotonated with a freshly prepared ethanolic solution of sodium ethoxide (4 equiv for **1**−**7** and 2 equiv for **8**). The NaCl precipitate was filtered off, and the filtrate was treated with 2 equiv of 2-acetylpyridine. The colorless solutions were stirred for 24 h, during which time they became yellow-orange, owing to the Schiff base formation. The ligands were not further purified, and the resulting ethanolic solutions were deoxygenated prior to use for complexation reactions.

Complexes. All complexation reactions and sample preparations for physical measurements were carried out in a purified nitrogen atmosphere within a glovebox (Vacuum Atmospheres H.E.43.2) equipped with a dry train (Jahan EVAC 7).

General Procedure (1−4). To a vigorously stirred solution of $Fe(O_2CMe)_2 \cdot 2H_2O$ (**1**, **2**, 0.43 g, 2.06 mmol; **3**, 0.82 g, 3.88 mmol; **4**, 0.88 g, 4.20 mmol) in MeOH (10 mL) was added a solution of acpypentOH (**1**, **2**, 1.03 mmol; **3**, 1.94 mmol; **4**, 2.10 mmol) in EtOH (**1**, **2**, 30 mL; **3**, **4**, 40 mL). The color of the solution turned immediately to dark blue, and then, a solution of pseudohalide salt was added (**1**, KSCN 0.20 g, 2.06 mmol; **2**, KSeCN 0.30 g, 2.06 mmol; **3**, KOCN 0.32 g, 3.88 mmol; **4**, NaN_3 0.27 g, 4.20 mmol) in MeOH (**1**, **2**, 10 mL; **3**, **4**, 20 mL). The solutions were filtered and left undisturbed for 24 h. The crystalline solids obtained were washed with a small quantity of MeOH and dried in vacuo.

General Procedure (5−7). To a vigorously stirred solution of $Fe(O_2CMe)_2 \cdot 2H_2O$ (**5**, 0.33 g, 1.56 mmol; **6**, 0.20 g, 0.96 mmol; **7**, 0.34 g, 1.63 mmol) in MeOH (3 mL) was added a solution of acpybutOH (**5**, 0.70 mmol; **6**, 0.46 mmol; **7**, 0.73 mmol) in EtOH (12 mL). The color of the solution turned immediately to very dark blue, and then, a solution of pseudohalide salt (**5**, KSCN 0.15 g, 1.56 mmol; **6**, KOCN 0.078 g, 0.96 mmol; **7**, NaN_3 0.11 g, 1.63 mmol) in MeOH (5 mL) was added. The solutions were filtered and left undisturbed for 24 h. The crystalline or microcrystalline solids obtained were washed with a small quantity of MeOH and dried in vacuo.

$[Fe_2(acpypentO)(O_2CMe)(NCS)_2]$ (1). Dark blue prismatic crystals. Yield: 0.271 g (∼ 54%). Anal. Calcd for $C_{23}H_{26}Fe_2N_6O_3S_2$: C, 45.26; H, 4.29; N, 13.77; Fe, 18.30. Found: C, 45.40; H, 4.26; N, 13,45; Fe, 18.14. IR data (KBr pellet, cm^{-1}): 2076 (vs, $\nu_{C=N}$), 1594 (s, ν_{asOAc}), 1437 (s, ν_{sOAc}).

$[Fe_2(acpypentO)(O_2CMe)(NCSe)_2]$ (2). Dark blue crystalline solid. Yield: 0.171 g (∼23%). Anal. Calcd for $C_{23}H_{26}Fe_2N_6O_3Se_2$: C, 39.23; H, 3.72; N, 11.94; Fe, 15.86. Found: C, 39.14; H, 3.30; N, 11.72; Fe, 15.29. IR data (KBr pellet, cm^{-1}): 2091, 2078 (vs, $\nu_{C=N}$), 1594 (s, ν_{asOAc}), 1438 (s, ν_{sOAc}).

$[Fe_2(acpypentO)(NCO)_3]$ (3). Dark blue prismatic crystals. Yield: 0.23 g (∼32% based on KOCN). Anal. Calcd for $C_{22}H_{23}Fe_2N_7O_4$: C, 47.01; H, 4.13; N, 17.47; Fe, 19.90. Found: C, 47.20; H, 4.19; N, 17.10; Fe, 19.49. IR data (KBr pellet, cm^{-1}): 2203, 2175 (vs, $\nu_{C=N}$).

$[Fe_4(acpypentO)_2(N_3)_6]$ (4). Dark blue prismatic crystals. Yield: 0.070 g (∼4% based on NaN_3). Anal. Calcd for $C_{38}H_{46}Fe_4N_{26}O_2$: C, 40.67; H, 4.13; N, 32.45; Fe, 19.90. Found: C, 40.60; H, 3.89; N, 31.81; Fe, 19.49. IR data (KBr pellet, cm^{-1}): 2046 (vs, $\nu_{N=N}$).

$[Fe_2(acpybutO)(O_2CMe)(NCS)_2]$ (5). Dark blue prismatic crystals. Yield: 0.174 g (∼37%). The dried sample analyzed as **5**·MeOH. Anal. Calcd for $C_{23}H_{28}Fe_2N_6O_4S_2$: C, 44.88; H, 4.71; N, 13.08; Fe, 17.78. Found: C, 44.73; H, 4.58; N, 12.98; Fe, 17.50. IR data (KBr pellet, cm^{-1}): 2069 (vs, $\nu_{C=N}$), 1567 (s, ν_{asOAc}), 1430 (s, ν_{sOAc}).

$[Fe_2(acpybutO)(O_2CMe)(NCO)_2]$ (6). Dark blue plates that formed after 24 h were collected by filtration, washed with a small amount of MeOH, and dried in vacuo. Yield: 0.081 g (∼32%). The dried sample analyzed as **6**·0.5MeOH. Anal. Calcd for $C_{22.5}H_{26}Fe_2N_7O_{4.5}$: C, 46.58; H, 4.52; N, 14.49; Fe, 19.80. Found: C, 46.31; H, 4.29; N, 14.39; Fe, 19.42. IR data (KBr pellet, cm^{-1}): 2203 (vs, $\nu_{C=N}$), 1547 (s, ν_{asOAc}), 1438 (s, ν_{sOAc}).

$[Fe_2(acpybutO)(O_2CMe)(N_3)_2]$ (7). Dark blue needles. Yield: 0.137 g (∼30%). Anal. Calcd for $C_{20}H_{24}Fe_2N_{10}O_3$: C, 42.58; H, 4.29; N, 24.83; Fe, 19.80. Found: C, 42.11; H, 4.08; N, 24.69; Fe, 19.55. IR data (KBr pellet, cm^{-1}): 2058 (vs, $\nu_{N=N}$), 1557 (s, ν_{asOAc}), 1424 (s, ν_{sOAc}).

$[Fe(acpybutOH)(NCS)_2]$ (8). To a vigorously stirred yellow-orange solution of acpybutOH (0.99 mmol) in EtOH (9 mL) was slowly added a colorless solution of $Fe(O_2CMe)_2 \cdot 2H_2O$ (0.19 g, 0.90 mmol) in MeOH (3 mL). The color immediately changed to very dark blue, and then, a solution of KSCN (0.18 g, 1.80 mmol) in MeOH (3 mL) was added. The resulting solution was filtered and left undisturbed for 24 h. Dark blue crystals that formed were collected by filtration, washed with a small amount of MeOH, and dried in vacuo. Yield: 0.084 g (∼19%). Anal. Calcd for $C_{20}H_{21}FeN_6OS_2$: C, 49.90; H, 4.40; N, 17.46; Fe, 11.60. Found: C, 49.98; H, 4.63; N, 17.28; Fe, 11.51. IR data (KBr pellet, cm^{-1}): 2119 (vs, $\nu_{C=N}$).

Crystallographic Data Collection and Structure Determination for 1, 3, 4·MeOH, and 8·MeOH. The selected crystals of **1** (blue-black plate, 0.50 × 0.25 × 0.10 mm^3), **3** (blue-black plate, 0.40 × 0.25 × 0.10 mm^3), **4**·MeOH (black parallelepiped, 0.30 × 0.20 × 0.15 mm^3), and **8**·MeOH (blue-black plate, 0.50 × 0.20 × 0.10 mm^3) were mounted on a Stoe imaging plate diffractometer system (IPDS) using a graphite monochromator ($\lambda = 0.71073$ Å) and equipped with an Oxford Cryosystems cooler device. The data were collected at 180 K for **1**, **3**, and **8**·MeOH and 160 K for **4**·MeOH. The crystal-to-detector distance was 70 mm (max 2θ value 52.1°) for **1**, **3**, and **8**·MeOH and 80 mm (max 2θ value 48.4°) for **4**·MeOH. Data were collected[15] with a φ oscillation movement ($\varphi = 0.0-202.8°$, $\Delta\varphi = 1.2°$ for **1**, $\varphi = 0.0-250.6°$, $\Delta\varphi = 1.4°$ for **3**, $\varphi = 0.0-250.6°$, $\Delta\varphi = 1.4°$ for **4**·MeOH, and $\varphi = 0.0-250.8°$, $\Delta\varphi = 1.9°$ for **8**·MeOH). There were 21502 reflections collected for **1**, of which 5363 were independent ($R_{int} = 0.0393$), 11599 reflections collected for **3**, of which 4318 were independent ($R_{int} = 0.0401$), 10702 reflections collected for **4**·MeOH, of which 3920 were independent ($R_{int} = 0.0381$), and 11514 reflections collected

(12) Boinnard, D.; Cassoux, P.; Petrouleas, V.; Savariault, J.-M.; Tuchagues, J.-P. *Inorg. Chem.* **1990**, *29*, 4114.
(13) Murase, I.; Hatano, M.; Tanaka, M.; Ueno, S.; Okawa, H.; Kida, S. *Bull. Chem. Soc. Jpn.* **1982**, *55*, 2204.
(14) Murase, I.; Ueno, S.; Kida, S. *Inorg. Chim. Acta* **1984**, *87*, 155.
(15) *IPDS Manual*, version 2.93; Stoe & Cie: Darmstadt, Germany, 1997.

Table 1. Crystallographic Data Collection and Structure Determination

	1	**3**	**4**·MeOH	**8**·MeOH
formula	$C_{23}H_{26}Fe_2N_6O_3S_2$	$C_{22}H_{23}Fe_2N_7O_4$	$C_{39}H_{50}Fe_4N_{26}O_3$	$C_{21}H_{26}FeN_6O_2S_2$
fw	610.32	561.17	1154.45	514.45
space group	$P2_1/n$ (No. 14)	$P\bar{1}$ (No. 2)	$P\bar{1}$ (No. 2)	$P\bar{1}$ (No. 2)
a, Å	8.0380(7)	8.4152(10)	9.1246(11)	8.7674(9)
b, Å	12.4495(8)	9.1350(10)	10.2466(11)	12.0938(13)
c, Å	27.358(2)	17.666(2)	14.928(2)	12.2634(14)
α, deg	90.0	97.486(14)	91.529(15)	106.685(14)
β, deg	92.180(10)	100.026(14)	101.078(16)	93.689(14)
γ, deg	90.0	113.510(13)	106.341(14)	108.508(13)
V, Å^3	2735.7(4)	1195.9(2)	1309.6(3)	1163.7(2)
Z	4	2	1	2
ρ_{calcd}, g cm^{-3}	1.482	1.558	1.464	1.468
λ, Å	0.71073	0.71073	0.71073	0.71073
T, K	180	180	160	180
μ(Mo Kα), cm^{-1}	12.49	12.57	11.49	8.58
$R_{(obs,all)}$[a]	0.0333, 0.0358	0.0324, 0.0432	0.0250, 0.0264	0.0388, 0.0416
$R_{w(obs,all)}$[b]	0.0668, 0.0672	0.0728, 0.0753	0.0504, 0.0509	0.0924, 0.0932

[a] $R = \sum||F_o| - |F_c||/\sum|F_o|$. [b] $R_w = [\sum w(|F_o|^2 - |F_c|^2)^2/\sum w|F_o^2|^2]^{1/2}$.

for **8**·MeOH, of which 4259 were independent (R_{int} = 0.0431). Numerical absorption corrections[16] were applied to **1** (T_{max} = 0.8783, T_{min} = 0.5671), to **3** (T_{max} = 0.6256, T_{min} = 0.3723) and to **8**·MeOH (T_{max} = 0.6909, T_{min} = 0.3778). The structures were solved by direct methods using SHELXS-97[17] and refined by full-matrix least-squares on F_o^2 with SHELXL-97.[18] All non-hydrogen atoms were refined anisotropically. H atoms were introduced in calculations by using the riding model with U_{iso} = 1.1*U*(atom of attachment). The atomic scattering factors and anomalous dispersion terms were taken from the standard compilation.[19] The maximum and minimum peaks on the final difference Fourier map were 0.323 and −0.359 e Å^{-3} for **1**, 0.458 and −0.350 e Å^{-3} for **3**, 0.311 and −0.312 e Å^{-3} for **4**·MeOH, and 0.304 and −0.500 e Å^{-3} for **8**·MeOH, respectively. Drawings of the molecules were performed with the program ORTEP.[20] Crystal data collection and refinement parameters are collected in Table 1, and selected bond distances and angles are gathered in Table 2 for **1**, Table 3 for **3**, Table 4 for **4**·MeOH, and Table 5 for **8**·MeOH.

Physical Measurements. Microanalyses for C, H, and N were performed by the Microanalytical Laboratory of the Laboratoire de Chimie de Coordination at Toulouse and at the Service Central de Microanalyses du CNRS in Vernaison, France, for Fe. Infrared spectra (4000−400 cm^{-1}) were recorded as KBr disks on a Perkin-Elmer Spectrum GX FT-IR spectrometer. Mössbauer measurements were recorded on a constant acceleration conventional spectrometer with a 50 mCi source of ^{57}Co (Rh matrix). The absorber was a powdered sample enclosed in a 20 mm diameter cylindrical, plastic sample-holder, the size of which had been determined to optimize the absorption. Variable-temperature spectra were obtained in the 80−300 K range, by using an MD 306 Oxford cryostat, the thermal scanning being monitored by an Oxford ITC4 servocontrol device (±0.1 K accuracy). A least-squares computer program[21] was used to fit the Mössbauer parameters and determine their standard deviations of statistical origin (given in parentheses). Isomer shift values (δ) are relative to iron foil at 293 K. Variable temperature (2−300 K) magnetic susceptibility data were collected on powdered microcrystalline solids on a Quantum Design MPMS SQUID susceptometer. Data were corrected with the standard procedure for the contribution of the sample holder and diamagnetism of the sample. The magnetic susceptibility has been computed by exact calculation of the energy levels associated with the spin Hamiltonian through diagonalization of the full matrix with a general program

Table 2. Selected Bond Lengths (Å) and Angles (deg) for Complex 1

Fe(1)−O(1)	2.0476(14)	Fe(2)−O(2)	2.0614(14)
Fe(1)−O(3)	1.9998(13)	Fe(2)−O(3)	1.9958(14)
Fe(1)−N(1)	2.1762(17)	Fe(2)−N(3)	2.1972(18)
Fe(1)−N(2)	2.1402(17)	Fe(2)−N(4)	2.1229(17)
Fe(1)−N(5)	2.0911(18)	Fe(2)−N(6)	2.0949(18)
Fe(1)···Fe(2)	3.287		
O(1)−Fe(1)−O(3)	106.08(6)	O(2)−Fe(2)−O(3)	106.60(6)
O(1)−Fe(1)−N(1)	83.02(6)	O(2)−Fe(2)−N(3)	83.63(6)
O(1)−Fe(1)−N(2)	157.71(6)	O(2)−Fe(2)−N(4)	157.25(6)
O(1)−Fe(1)−N(5)	95.36(7)	O(2)−Fe(2)−N(6)	95.58(6)
O(3)−Fe(1)−N(1)	156.07(6)	O(3)−Fe(2)−N(3)	152.58(6)
O(3)−Fe(1)−N(2)	91.84(6)	O(3)−Fe(2)−N(4)	91.67(6)
O(3)−Fe(1)−N(5)	98.84(6)	O(3)−Fe(2)−N(6)	100.99(6)
N(1)−Fe(1)−N(2)	75.47(7)	N(3)−Fe(2)−N(4)	74.11(7)
N(1)−Fe(1)−N(5)	102.34(7)	N(3)−Fe(2)−N(6)	103.26(7)
N(2)−Fe(1)−N(5)	94.84(7)	N(4)−Fe(2)−N(6)	94.06(7)
Fe(1)−O(3)−Fe(2)	110.69(6)		

Table 3. Selected Bond Lengths (Å) and Angles (deg) for Complex **3**

Fe(1)−O(1)	1.9700(17)	Fe(2)−O(1)	2.0409(19)
Fe(1)−N(1)	2.1587(19)	Fe(2)−N(3)	2.142(2)
Fe(1)−N(2)	2.128(2)	Fe(2)−N(4)	2.146(2)
Fe(1)−N(5)	2.167(2)	Fe(2)−N(5)	2.1638(18)
Fe(1)−N(6)	1.997(2)	Fe(2)−N(7)	1.974(3)
Fe(1)···Fe(2)	3.172		
O(1)−Fe(1)−N(1)	137.11(7)	O(1)−Fe(2)−N(3)	87.23(8)
O(1)−Fe(1)−N(2)	90.12(8)	O(1)−Fe(2)−N(4)	140.43(8)
O(1)−Fe(1)−N(5)	81.21(7)	O(1)−Fe(2)−N(5)	79.72(7)
O(1)−Fe(1)−N(6)	117.50(9)	O(1)−Fe(2)−N7	112.20(10)
N(1)−Fe(1)−N(2)	74.91(9)	N(3)−Fe(2)−N(4)	75.10(8)
N(1)−Fe(1)−N(5)	95.94(8)	N(3)−Fe(2)−N(5)	144.60(8)
N(1)−Fe(1)−N(6)	104.77(9)	N(3)−Fe(2)−N7	108.54(10)
N(2)−Fe(1)−N(5)	155.44(8)	N(4)−Fe(2)−N(5)	94.46(7)
N(2)−Fe(1)−N(6)	100.29(9)	N(4)−Fe(2)−N7	106.97(10)
N(5)−Fe(1)−N(6)	104.11(9)	N(5)−Fe(2)−N7	106.85(10)
Fe(1)−O(1)−Fe(2)	104.53(8)	Fe(1)−N(5)−Fe(2)	94.21

(16) *X.-SHAPE, Crystal Optimisation for Numerical Absorption Correction*, revision 1.01; Stoe & Cie: Darmstadt, Germany, 1996.
(17) Sheldrick, G. M. *SHELXS-97. Program for Crystal Structure Solution*; University of Göttingen: Göttingen, Germany, 1990.
(18) Sheldrick, G. M. *SHELXL-97. Program for the refinement of crystal structures from diffraction data*; University of Göttingen: Göttingen, Germany, 1997.
(19) *International Tables for Crystallography*; Kluwer Academic Publishers: Dordrecht, The Netherlands, 1992; Vol. C, Tables 4.2.6.8 and 6.1.1.4.
(20) ORTEP32 for Windows: Farrugia, L. J. *J. Appl. Crystallogr.* **1997**, *30*, 565.
(21) Lagarec, K. *Recoil, Mössbauer Analysis Software for Windows*; http://www.physics.uottawa.ca/~recoil.

Table 4. Selected Bond Lengths (Å) and Angles (deg) for Complex **4**

Fe(1)−O(1)	1.9578(9)	Fe(2)−O(1)	2.0261(9)
Fe(1)−N(1)	2.1336(11)	Fe(2)−N(3)	2.1385(11)
Fe(1)−N(2)	2.1405(9)	Fe(2)−N(4)	2.1152(10)
Fe(1)−N(5)	2.2733(11)	Fe(2)−N(5)	2.1168(11)
Fe(1)−N(8)	2.1669(9)	Fe(2)−N(11)	1.9922(11)
Fe(1)−N(8′)	2.2043(10)	Fe(1)···Fe(1′)	3.3511(4)
Fe(1)···Fe(2)	3.1968(2)		
O(1)−Fe(1)−N(1)	158.26(4)	N(1)−Fe(1)−N(8)	93.96(4)
O(1)−Fe(1)−N(2)	90.60(4)	N(1)−Fe(1)−N(8′)	93.37(4)
O(1)−Fe(1)−N(5)	78.43(4)	N(2)−Fe(1)−N(5)	107.40(4)
O(1)−Fe(1)−N(8)	103.65(4)	N(2)−Fe(1)−N(8)	162.11(4)
O(1)−Fe(1)−N(8′)	102.10(4)	N(2)−Fe(1)−N(8′)	86.65(4)
N(1)−Fe(1)−N(2)	74.99(4)	N(5)−Fe(1)−N(8)	86.31(4)
N(1)−Fe(1)−N(5)	90.26(4)	N(5)−Fe(1)−N(8′)	165.95(3)
N(8)−Fe(1)−N(8′)	79.90(4)	N(3)−Fe(2)−N(5)	145.42(4)
O(1)−Fe(2)−N(3)	81.06(4)	N(3)−Fe(2)−N(11)	114.86(4)
O(1)−Fe(2)−N(4)	134.86(4)	N(4)−Fe(2)−N(5)	98.84(4)
O(1)−Fe(2)−N(5)	80.81(4)	N(4)−Fe(2)−N(11)	107.96(4)
O(1)−Fe(2)−N(11)	116.65(4)	N(5)−Fe(2)−N(11)	99.57(4)
N(3)−Fe(2)−N(4)	74.28(4)	Fe(1)−O(1)−Fe(2)	106.71(4)
Fe(1)−N(8)−Fe(1′)	100.10(4)	Fe(1)−N(5)−Fe(2)	93.40(4)

Table 5. Selected Bond Lengths (Å) and Angles (deg) for Complex **4**

Fe−N(1)	1.9293(18)	Fe−N(4)	1.9266(17)
Fe−N(2)	1.9565(17)	Fe−N(5)	1.9583(19)
Fe−N(3)	1.9565(17)	Fe−N(6)	1.9587(19)
N(1)−Fe−N(2)	80.99(7)	N(2)−Fe−N(5)	91.30(7)
N(1)−Fe−N(3)	96.16(8)	N(2)−Fe−N(6)	94.90(7)
N(1)−Fe−N(4)	92.83(7)	N(3)−Fe−N(4)	81.05(7)
N(1)−Fe−N(5)	87.21(7)	N(3)−Fe−N(5)	93.36(7)
N(1)−Fe−N(6)	173.10(7)	N(3)−Fe−N(6)	88.39(8)
N(2)−Fe−N(3)	174.41(7)	N(4)−Fe−N(5)	174.38(7)
N(2)−Fe−N(4)	94.25(7)	N(4)−Fe−N(6)	93.01(7)
N(5)−Fe−N(6)	87.33(8)		

for axial symmetry.[2] Least-squares fittings were accomplished with an adapted version of the function-minimization program MINUIT.[22]

Results and Discussion

Syntheses. The reactions yielding the acetato bridged dinuclear complexes (**1**, **2**, **5**−**7**) may be summarized by eq 1, and those yielding complexes **3** and **4** by eqs 2 and 3, respectively. It should be noted that all these reactions were carried out with an excess of EtONa, in order to induce deprotonation of the central alcoholic function of the ligands, leading to alkoxo bridged species.

$$2Fe(O_2CMe)_2\cdot 2H_2O + LNa + 2\,(K, Na)X \xrightarrow{MeOH,\ EtOH} [Fe_2(O_2CMe)(L)(X)_2] + MeCO_2Na + 2MeCO_2Na + 2MeCO_2(K, Na)\ (L = acpypentO^-, acpybutO^-) \quad (1)$$

$$2Fe(O_2CMe)_2\cdot 2H_2O + acpypentONa + 3KOCN \xrightarrow{MeOH,\ EtOH} [Fe_2(acpypentONa)(NCO)_3] + MeCO_2Na + 3MeCO_2K \quad (2)$$

For the acpypentO bridged complexes, we observe that the nature of the complex depends on the pseudohalide anion. For NCS^- (**1**) and $NCSe^-$ (**2**), the resulting complexes

$$4Fe(O_2CMe)_2\cdot 2H_2O + 2acpypentONa + 6NaN_3 \xrightarrow{MeOH,\ EtOH} [Fe_2(acpypentO)(N_3)_3]_2 + 8MeCO_2Na \quad (3)$$

contain an additional syn, syn η^1:η^1:μ_2 syn:syn acetato bridge, whereas for NCO^- (**3**) the additional bridge is provided by an end-on cyanato anion. In the case of **4**, which can be considered as a bis-dinuclear species, the additional intradinuclear bridge is provided by an end-on azido anion.

In the case of the acpybutO complexes, however, there is no dependence of the composition and structure on the pseudohalide anion; all complexes contain the syn, syn η^1:η^1:μ_2 syn:syn acetato bridge observed in complexes **1** and **2**. This conclusion is supported by a low resolution structure of complex **5** (not reported) which confirms the existence of the abovementioned bridge, but also by microanalytical results, and the close similarities of the spectral (IR, Mössbauer) and magnetic properties of complexes **1**, **2**, and **5**−**7** (see related sections).

The synthesis of the mononuclear complex **8** was initially serendipitous and occurred while trying to prepare complex **5** with an experimental procedure similar to that for **1**. The structure of the selected crystal was that of complex **8**. The Mössbauer spectrum of the microcrystalline solid showed one high-spin (HS) and one low-spin (LS) iron sites: their relative areas, independent of temperature, excluded the possibility of a spin-crossover compound.

Given the spontaneous formation of complex **8**, in order to obtain the dinuclear species **5**, we chose conditions that would strongly favor formation of the latter. Slow addition of the Schiff base to a ferrous acetate solution was employed, to ensure a constant excess of iron. In addition, the iron/acpybutOH ratio was restricted to 2:0.9 stoichiometry, in order to further favor formation of the dinuclear species, and the reaction was carried out with an excess of EtONa. The solid obtained under these conditions was crystallographically characterized as the dinuclear complex **5**, but the quality of the resolution was poor and therefore the structure is not reported. The Mössbauer spectrum showed the presence of two relatively similar HS Fe^{II} sites. There was, however, a ∼10% minor iron site with small isomer shift and quadrupole splitting which could be attributed either to HS Fe^{III} or to LS Fe^{II}. The similarity of the Mössbauer parameters of the minor site to those of complex **8** and the absence of EPR signal led us to the conclusion that the mononuclear complex is so stable that it forms even in conditions favoring the dinuclear species. Mössbauer spectra of **6** and **7** revealed the existence of similar minor LS Fe^{II} sites (5−10%).

The opposite strategy was employed to obtain pure **8**. Ferrous acetate was slowly added to the Schiff base solution, and the iron/acpybutOH/KSCN ratio was fixed to 1:1.1:2. In addition, a stoichiometric amount of EtONa was used to generate the neutral diamino alcohol from its dihydrochloride, therefore avoiding the deprotonated acpybutO during the complexation reaction. In this case, Mössbauer spectra showed only one LS Fe^{II} site and no trace of HS Fe^{II} site, as expected given the high stability of the mononuclear complex **8**. This reaction is summarized in eq 4.

(22) James, F.; Roos, M. MINUIT Program, a System for Function Minimization and Analysis of the Parameters Errors and Correlations. *Comput. Phys. Commun*. **1975**, *10*, 345.

$$Fe(O_2CMe)_2{\cdot}2H_2O + acpybutOH + 2KNCS \xrightarrow{MeOH,\ EtOH} [Fe(acpybutOH)(NCS)_2] + 2MeCO_2K \quad (4)$$

Attempts to synthesize the equivalent mononuclear complex with acpypentOH, i.e., [Fe(acpypentOH)(NCS)$_2$], yielded a dark purple solid, the Mössbauer spectrum of which indicated the presence of both LS and HS sites. Again, the relative areas of the peaks being independent of temperature, we concluded that the sample was a mixture of **1** and [Fe(acpypentOH)(NCS)$_2$].

From the above, the following general conclusions may be summarized for these systems: (i) For the acpypentOH ligand, the nature of the product strongly depends on the coordinated pseudohalide, whereas for the acpybutOH ligand, only acetato-bridged compounds are obtained. (ii) The coordinated pseudohalides can be grouped into two categories, according to the type of bridging they favor with acpypentOH: (a) NCS^- and $NCSe^-$ yielding acetato-bridged complexes, and (b) NCO^- and N_3^- yielding end-on pseudohalido-bridged complexes. (iii) The most stable acpypentOH complexes contain dinuclear motifs, even under conditions favoring formation of mononuclear products. Conversely, mononuclear acpybutOH complexes form, even under conditions favoring formation of dinuclear species.

On the basis of these results, a general outline may be suggested: the five-carbon backbone endows acpypentOH with a flexibility that enables a closer or farther approach of the bridged iron(II) atoms, allowing therefore the supplementary bridge to be either an end-on pseudohalide, with a smaller Fe···Fe separation (**3**, Fe1−Fe2, 3.172 Å; **4**, Fe1−Fe2, 3.196 Å), or an acetate with a larger Fe···Fe separation (**1**, Fe1−Fe2, 3.287 Å). Apparently, the four-carbon backbone of acpybutOH is too rigid to allow a close approach, and therefore, only acetato-bridged systems are allowed. In contrast, the four-carbon backbone of acpybutOH seems to be ideally sized to close a seven-membered ring including an iron(II) ion (**8**: N2−C7−C8−C9−C10−N4−Fe) and form a mononuclear complex, whereas the eight-membered ring of acpypentOH is apparently too unstable.

Description of Structures. ORTEP plots of complexes **1**, **3**, **4**, and **8** are shown in Figures 1, 2, 3, and 4, respectively. Selected interatomic distances and angles for complexes **1**, **3**, **4**, and **8** are listed in Tables 2, 3, 4, and 5, respectively.

Complex **1** includes two iron atoms bridged by one alkoxo and one syn, syn $\eta^1{:}\eta^1{:}\mu_2$ acetato. The coordination sphere of both iron sites is a distorted tetragonal pyramid. The trigonality index τ ($=(\phi_1 - \phi_2)/60$, where ϕ_1, ϕ_2 are the two largest L−M−L angles of the coordination sphere)[23] has been calculated for the two iron sites. $\tau = 0.027$ and 0.078 for sites Fe1 and Fe2, respectively, confirming the highly tetragonal pyramidal character of both sites ($\tau = 0$ infers a perfect square pyramid, and $\tau = 1$ a perfect trigonal bipyramid). Each pyramid base is defined by one pyridine donor and one imine nitrogen donor, the bridging alkoxo, and one acetate oxygen atom (N(1), N(2), O(3), and O(1), and N(3), N(4), O(3), and O(2) for Fe1 and Fe2, respectively). The apices, which are found at cis relative positions, are occupied by the NCS^- nitrogen atoms N5 and N6 for Fe1 and Fe2, respectively. The intermetallic Fe1···Fe2 separation is 3.287 Å, whereas the Fe1−O3−Fe2 angle is 110.69°.

The packing diagram of complex **1** (Figure SI1) reveals intermolecular interactions between atom S2 of the NCS^-

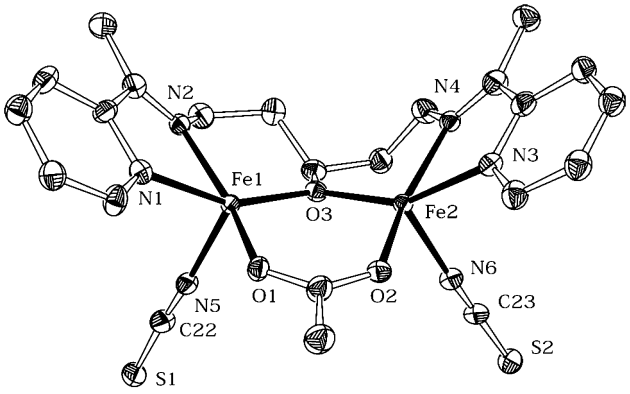

Figure 1. ORTEP plot of complex **1** at the 30% probability level.

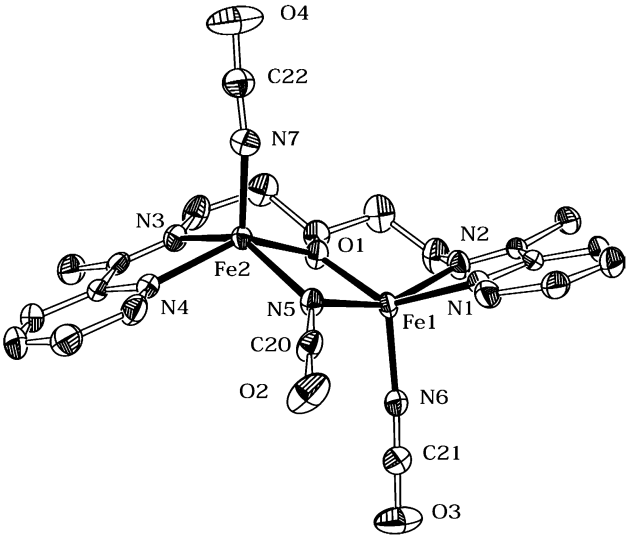

Figure 2. ORTEP plot of complex **3** at the 30% probability level.

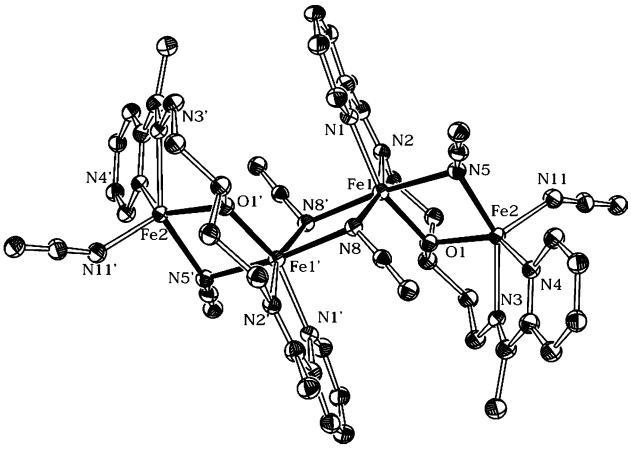

Figure 3. ORTEP plot of complex **4** at the 30% probability level.

(23) (a) Hathaway, B. J. *Struct. Bonding* **1973**, *14*, 49. (b) Addison, A. W.; Nageswara, T.; Reedijk, J.; van Rijn, J.; Verchoor, G. C. *J. Chem. Soc., Dalton Trans.* **1984**, 1349.

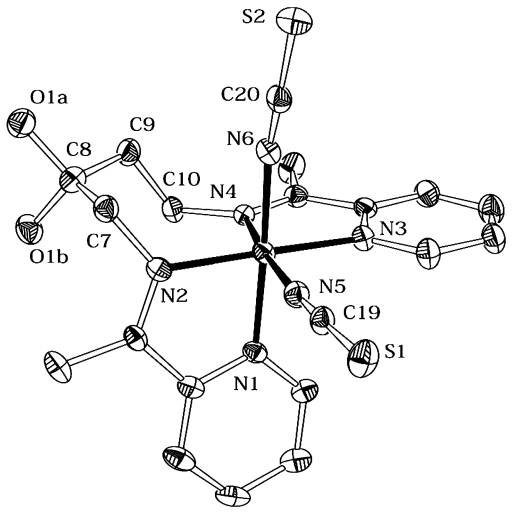

Figure 4. ORTEP plot of complex **8** at the 30% probability level.

terminal ligand and the two iron atoms Fe1′ and Fe2′ of a neighboring molecule ($' = -x + {}^1/_2, y + {}^1/_2, -z + {}^1/_2$). The S atom is situated directly above the vacant coordination sites of Fe1′ and Fe2′, and the distances S2···Fe1′ and S2···Fe2′ are 3.105 and 3.176 Å, respectively. The S2···Fe1′−N5′ (174.58°) and S2···Fe2′−N6′ (175.37°) angles are very close to 180°. Repetition of this motif results in 1D chains parallel to the *b* axis. This thiocyanato bridging mode has already been observed, the corresponding M−S distances being in the 2.6−2.9 Å range.[24] The M−S distance in complex **1** is significantly longer, suggesting weak Fe···S interactions, rather than covalent bonding.

Complex **3** (Figure 2) includes two iron(II) atoms, bridged by one alkoxo oxygen atom and one end-on cyanate anion. The coordination environment for both iron(II) atoms is tetragonal pyramidal; each pyramid base is defined by one pyridine and one imine nitrogen donors (N1 and N2, and N4 and N3 for Fe1 and Fe2, respectively), the bridging alkoxo-oxygen atom O1 and the nitrogen atom N5 of the end-on bridging cyanate. The apical positions of Fe1 and Fe2 are occupied by the nitrogen atoms of two terminally bound cyanates (N6 and N7, respectively). The intermetallic Fe1···Fe2 separation is 3.172 Å, and the angles formed between the metal centers and their monatomic bridges are 104.53° and 94.21° for Fe1−O1−Fe2 and Fe1−N5−Fe2, respectively.

Although the two sites appear to be relatively similar, the trigonality indices of Fe1 ($\tau = 0.31$) and Fe2 ($\tau = 0.07$) revealed important differences in geometry. The coordination sphere of Fe1 is endowed with a ∼31% trigonal bipyramidal character, whereas the coordination sphere of Fe2 has only 7% of such character: the rhombic distortion is thus much higher for Fe1 compared to Fe2.

Despite very similar general features, complexes **1** and **3** are distinguished by two prominent differences: (i) while the iron centers are acetato bridged in complex **1**, they are end-on μ_2-NCO bridged in complex **3**, and (ii) the apical terminally bound pseudohalides are in cis relative positions in complex **1** and in trans relative positions in complex **3**.

A packing diagram of complex **3** (Figure SI2) reveals the existence of intermolecular $\pi-\pi$ interactions. These can be divided into two types: (i) an interaction (∼3.9 Å) between the C1−C2−C3−C4−C5−N1 pyridine ring of one molecule with the C13−C14−C15−C16−C17−N4 pyridine ring of its symmetry counterpart (*x*, *y*, *z*) of the adjacent unit cell along *a*, and (ii) between two symmetry related (−*x*, −*y*, −*z*) C13−C14−C15−C16−C17−N4 pyridine rings of two adjacent unit cells along *a* (∼3.7 Å). The first type of $\pi-\pi$ interaction delineates 1D chains along *a*, whereas the second type connects two such chains along *c*, to form pairs: The lattice is thus made up of paralled pairs of 1D chains.

Complex **4** (Figure 3) includes four iron(II) atoms in a zigzag arrangement. Crystallographically, the complex consists of two dinuclear units, symmetry related by an inversion center situated between Fe1 and Fe1′. Each dinuclear unit consists of two iron(II) atoms bridged by the alkoxo oxygen O1 of the dinucleating Schiff base and one end-on azido anion. Interdinuclear connectivity is achieved by two end-on azido bridges between the symmetry related Fe1 and Fe1′atoms. There are two types of coordination geometries around iron: a tetragonal pyramidal one around the external metal centers (Fe2 and Fe2′) and an octahedral one around the internal (Fe1 and Fe1′) atoms. Restricting the description to one dinuclear unit, the pyramid base is defined by one pyridine nitrogen atom and one imine nitrogen atom (N4 and N3, respectively), one monatomic alkoxo bridge (O1), and one end-on azido bridge (N5). The apical position of the pyramid is occupied by one terminally bound azido nitrogen atom (N11). The trigonality index for Fe2 ($\tau = 0.18$) indicates a slight rhombic distortion. The coordination environment is similar for Fe1, bound to one pyridine nitrogen atom and one imine nitrogen atom (N1 and N2, respectively), one alkoxo oxygen atom (O1), and the end-on azido nitrogen atom N5. In the latter case, though, the coordination sphere is completed not by one terminal, but by two bridging end-on azido nitrogen atoms (N8 and N8′), and thus the geometry around Fe1 is octahedral.

The interdinuclear Fe1···Fe1′ separation is 3.351 Å, whereas the Fe1−N8−Fe1′−N8′ ring is planar due to symmetry, with Fe1−N8−Fe1′ and Fe1−N8′−Fe1′ angles equal to 100.10°. The intradinuclear Fe1···Fe2 separation is 3.197 Å, and the Fe1−N5−Fe2 and Fe1−O1−Fe2 angles are 93.40° and 106.71°, respectively. The ring, however, is not planar, and the Fe1−N5−Fe2−O1 dihedral angle equals 5.6°.

The iron(II) coordination sphere of complex **8** (Figure 4) is slightly distorted octahedral, with two imine (N2, N4), two pyridine (N1, N3), and two thiocyanato (N5, N6) nitrogen donors. The tetradentate acpybutOH ligand imposes coordination of the thiocyanate anions at cis positions of the octahedron. The Fe−N bond lengths span a very narrow range (∼1.93−1.96 Å) whereas the cis N−Fe−N angles span the 81−94° range, mainly due to stereochemical constraints

(24) (a) Vicente, R.; Escuer, A.; Peñalba, E.; Solans, X.; Font-Bardia, M.; *Inorg. Chim. Acta* **1997**, *255*, 7. (b) Gómez-Saiz, P.; García-Tojal, J.; Arnáiz, F. J.; Maestro, M. J.; Lezama, L.; Rojo, T. *Inorg. Chem. Commun.* **2003**, *6*, 558. (c) Maji, T. K.; Mostafa, G.; Clemente-Juan, J. M.; Ribas, J.; Lloret, F.; Okamoto, K.; Chaudhuri, N. R. *Eur. J. Inorg. Chem.* **2003**, 1005.

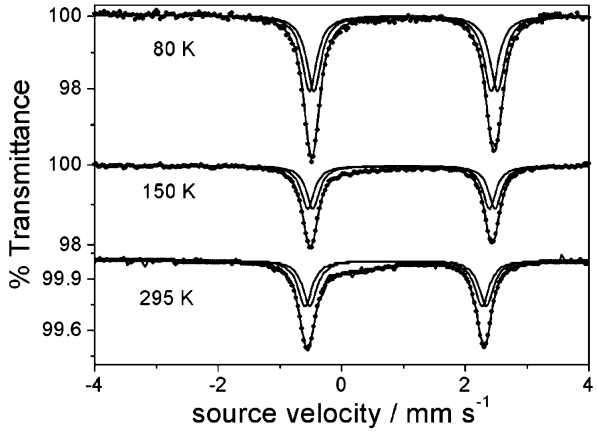

Figure 5. Variable-temperature ^{57}Fe Mössbauer spectra of complex **2**.

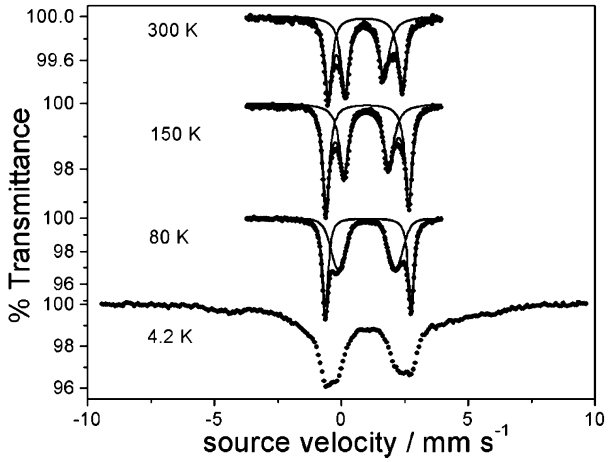

Figure 6. Variable-temperature ^{57}Fe Mössbauer spectra of complex **3**.

imposed by the ligand. The N1−Fe−N2 and N3−Fe−N4 angles deviate most from 90° (81.99 and 81.05°, respectively), the rest being in the 87−94° range. The trans N−Fe−N angles span the narrow 173.10−174.41° range.

The effect of the chirality of the ligand deserves some comments. The crystal structure shows two oxygen atoms (O1a and O1b) bound to the carbon atom C8. Since the two arms of the ligand are inequivalent, carbon atom C8, bound to four different substituents, is chiral. In the present syntheses, the ligand, prepared from *rac*-1,4-dibromo-butan-2-ol, was a racemic mixture of the two enantiomers. Thus, complex molecules with either enantiomeric Schiff base formed and syncrystallized, yielding crystals where half complex molecules contain the *R* conformer, and the other half contain the *S* one. Crystallographically, only one complex molecule was observed, with the alcoholic oxygen atom statistically distributed among positions O1a and O1b.

Mössbauer Spectroscopy. An overall inspection of the Mössbauer spectra of complexes **1**−**7** reveals that all acetato bridged complexes **1**, **2**, and **5**−**7** have the same overall features. Characteristic variable-temperature spectra of complex **1** are shown in Figure 5. Mössbauer spectra of complexes **3**, **4**, and **8** present different characteristic features and are examined separately. The spectra of **3** and **4** are depicted in Figures 6 and 7, respectively. Selected Mössbauer parameters are presented in Table 6 for all complexes.

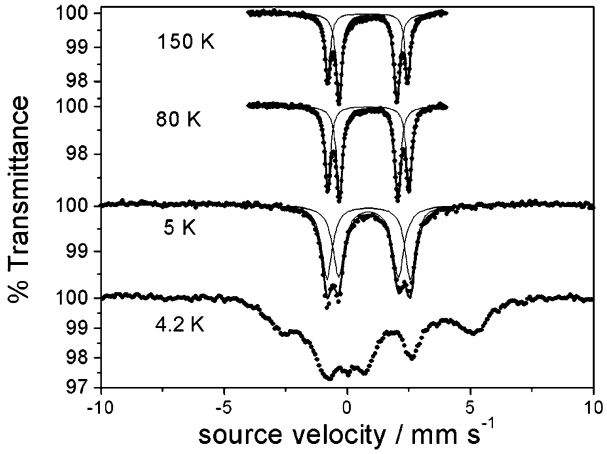

Figure 7. Variable-temperature ^{57}Fe Mössbauer spectra of complex **4**.

All acetato bridged dinuclear complexes present composite high-spin iron(II) quadrupole split doublets indicating the presence of two slightly different ferrous sites. The crystal structure of **1** and the low resolution structure of **5** evidence the presence of two iron sites with the same N_3O_2 donor set, but slightly different ligand environment geometries. Consequently, the spectra of complexes **1**, **2**, and **4**−**7** have been fitted with two quadrupole-split doublets of equal relative areas. It should be noted that efforts to fit with a single quadrupole split doublet gave poor results: asymmetries in the shape of the absorptions could not be accounted for. The derived parameters are in agreement with high-spin iron(II) sites characterized by similar isomer shifts and different quadrupole splittings, consistent with low symmetry environments.[12,25] In the case of complexes **5**−**7**, the Mössbauer spectra were actually fitted with three quadrupole-split doublets, two majority HS doublets of equal area, and one minority LS doublet (3−10%) corresponding to the mononuclear impurity mentioned in the Syntheses subsection: only the Mössbauer parameters of the two majority HS doublets have been collated in Table 6, yielding equal relative areas lower than 50%.

The Mössbauer spectra of complex **3** (Figure 6) consist of two well resolved quadrupole-split asymmetric doublets, as a result of the differences in local coordination geometries around Fe1 and Fe2. These doublets present relatively similar isomer shifts, of ∼1 mm s^{-1}, in agreement with similar coordination environments around the two iron(II) sites and quite different ΔE_Q values (∼3.4 mm s^{-1} and ∼2.3 mm s^{-1} at 80 K). The isomer shift values slightly decrease with increasing temperature, indicating operation of second-order Doppler effect.[26] The doublet with the largest ΔE_Q value is attributed to the more axially distorted site, i.e., Fe2 (see

(25) (a) Martinez Lorente, M. A.; Petrouleas, V.; Savariault, J.-M.; Poinsot, R.; Drillon, M.; Tuchagues, J.-P. *Inorg. Chem.* **1991**, *30*, 3587. (b) Rakotonandrasana, A. S.; Boinnard, D.; Petrouleas, V.; Cartier, C.; Verdaguer, M.; Savariault, J.-M.; Tuchagues, J.-P. *Inorg. Chim. Acta* **1991**, *180*, 19. (c) Martinez Lorente, M. A.; Dahan, F.; Petrouleas, V.; Bousseksou, A.; Tuchagues, J.-P. *Inorg. Chem.* **1995**, *34*, 5346. (d) Bernal, I.; Jensen, I. M.; Jensen, K. B.; McKenzie, C. J.; Toftlund, H.; Tuchagues, J.-P. *J. Chem. Soc., Dalton Trans.* **1995**, 3667. (e) Hemmert, C.; Verelst, M.; Tuchagues, J.-P. *J. Chem. Soc., Chem. Commun.* **1996**, 617. (f) Costes, J.-P.; Clemente-Juan, J. M.; Dahan, F.; Dumestre, F.; Tuchagues, J.-P. *Inorg. Chem.* **2002**, *41*, 2886.

Table 6. Mössbauer Parameters of Complexes **1**−**8**[a]

iron site	T (K)	δ[b] (mm s^{-1})	ΔE_Q (mm s^{-1})	$\Gamma_{1/2}$ (mm s^{-1})	surface (%)
1a (N_3O_2)[c]	80	1.081(1)	3.016(3)	0.120(2)	50
	150	1.052(9)	2.986(3)	0.112(1)	50
	293	0.971(2)	2.859(6)	0.117(2)	50
1b (N_3O_2)[c]	80	1.077(1)	2.799(3)	0.120(2)	50
	150	1.045(9)	2.804(3)	0.112(1)	50
	293	0.962(2)	2.723(6)	0.117(2)	50
2a (N_3O_2)[c]	80	1.091(2)	2.935(8)	0.136(3)	50
	150	1.059(1)	2.921(4)	0.121(2)	50
	295	0.968(3)	2.83(1)	0.131(4)	50
2b (N_3O_2)[c]	80	1.078(2)	2.771(8)	0.136(3)	50
	150	1.054(1)	2.752(4)	0.121(2)	50
	295	0.974(3)	2.68(1)	0.131(4)	50
3 (Fe(2), N_4O)	80	1.01(1)	3.375(3)	0.12(1)	46.0(1)
	150	1.031(1)	3.256(1)	0.171(1)	52.6(1)
	300	0.947(1)	2.910(1)	0.204(1)	49(1)
3 (Fe(1), N_4O)	80	1.01(1)	2.27(1)	0.49(1)	54.0(1)
	150	0.990(1)	1.775(1)	0.242(1)	47.5(1)
	300	0.913(1)	1.54(1)	0.25(1)	51(1)
4 (Fe(1), N_5O)	5	1.000(4)	2.46(1)	0.283(9)	51(2)
	80	1.007(1)	2.437(2)	0.149(2)	54.3(5)
	150	0.981(1)	2.419(3)	0.147(2)	59.4(7)
4 (Fe(2), N_4O)	5	1.007(4)	3.44(1)	0.259(9)	49(2)
	80	1.001(1)	3.398(2)	0.142(2)	45.7(5)
	150	0.972(2)	3.342(3)	0.133(3)	40.6(7)
5a (N_3O_2)[c]	80	1.045(1)	2.930(3)	0.137(2)	48.8(3)
	150	1.010(2)	2.886(8)	0.137(4)	47.0(5)
	300	0.927(8)	2.71(2)	0.14(1)	46(1)
5b (N_3O_2)[c]	80	1.031(1)	2.697(3)	0.137(2)	48.8(3)
	150	1.000(2)	2.688(8)	0.137(4)	47.0(5)
	300	0.955(8)	2.49(2)	0.14(1)	46(1)
6a (N_3O_2)[c]	80	1.044(3)	3.081(8)	0.147(3)	47.7(3)
	150	1.024(1)	2.961(3)	0.145(3)	45.0(3)
	293	0.90(1)	2.66(3)	0.148(8)	44.2(8)
6b (N_3O_2)[c]	80	0.990(3)	2.850(8)	0.147(3)	47.7(3)
	150	0.959(1)	2.811(3)	0.145(3)	45.0(3)
	293	0.94(1)	2.49(3)	0.148(8)	44.2(8)
7a (N_3O_2)[c]	80	1.074(1)	2.856(5)	0.151(2)	48.2(2)
	150	1.049(1)	2.841(4)	0.151(2)	47.7(2)
	300	0.954(2)	2.762(7)	0.165(4)	46.1(3)
7b (N_3O_2)[c]	80	1.069(1)	2.623(5)	0.151(2)	48.2(2)
	150	1.040(1)	2.598(4)	0.151(2)	47.7(2)
	300	0.961(2)	2.490(7)	0.165(4)	46.1(3)
8 (N_6)	80	0.364(1)	0.601(2)	0.136(1)	100
	150	0.351(2)	0.604(3)	0.143(2)	100
	293	0.296(1)	0.567(1)	0.130(1)	100

[a] Standard deviations of statistical origin are given in parentheses. [b] Referenced to metallic iron foil at 293 K. [c] Relative surfaces of two peaks fixed to equality.

Description of Structures subsection). Fe1 which presents a significant rhombic distortion is associated to the doublet with the smaller ΔE_Q value. For both sites, ΔE_Q values show a significant decrease with increasing temperature in the 80−300 K range. From the magnitude of their quadrupole splitting, we may assume a singlet ground state for both iron sites. Increasing temperature leads to population of the low-lying excited states, which are close to the ground state due to the low symmetry of the sites and spin−orbit interactions. Another characteristic aspect of these spectra is the broad line width of the Fe1 doublet compared to the Fe2 one at all temperatures, this effect increasing with decreasing temperature. A possible rationale would be to consider that the atoms involved in both types of $\pi-\pi$ interactions, and particularly the stronger pairwise ones, namely Fe2, might give rise to an unusual Mössbauer behavior associated with the ligand field effect of these combined π-stackings.

Another interesting feature concerns the asymmetry observed between the two branches of each doublet, a feature more pronounced at higher temperatures. This asymmetry may be associated to the anisotropy of thermally populated higher magnetic states ($S_T = 3, 2, 1$).[27]

The Mössbauer spectra of complex **4** (Figure 7) present two well resolved quadrupole-split doublets typical of high-spin iron(II) with quite different ΔE_Q values ($\Delta E_{QA} = 3.398(2)$ mm s^{-1}, $\Delta E_{QB} = 2.437(2)$ mm s^{-1}at 80 K), but isomer shifts close to each other ($\delta_A = 1.001(1)$ mm s^{-1}, $\delta_B = 1.007(1)$ mm s^{-1} at 80 K). The quadrupole splitting values illustrate the differences in coordination geometries for the two sites (tetragonal pyramidal for Fe(2) (site A), and distorted octahedral for Fe(1) (site B). The quadrupole splitting value for the pentacoordinated iron site of **4** is very close to the value observed for the more axial site of complex **3**, in agreement with their similar slight rhombic distortion (see Description of Structures subsection). The proximity of the isomer shift values is in agreement with the similarity in nature of the donors to Fe(1) (N_5O) and Fe(2) (N_4O). Owing to their clear separation, it was not necessary to impose equality of the relative doublet areas. Deviations of the area fractions from the 1:1 ratio are attributed to the foreseeable difference in Debye temperatures between pyramidally and octahedrally coordinated iron sites. In addition, the recoil-free fractions (f) of the two sites should differ due to the differences in local bonding.[26] For the external sites, Fe2 and Fe2′, with N_4O donor sets including only four bonds to the rest of the molecule, a more flexible binding to the crystal lattice is expected compared to the internal sites, Fe1 and Fe1′, with N_5O donor sets including six bonds to the rest of the molecule. The ∼8% difference in U_{eq} values confirms the higher mobility of site Fe2 (Fe2′) in the crystal lattice compared to Fe1 (Fe1′), in agreement with the lower recoil-free fractions of Fe2 (Fe2′). Moreover, as temperature increases we might expect a faster decrease of the recoil-free fractions for Fe2 (Fe2′), as thermal energy will be more effectively transformed into thermal agitation; indeed, this is the case (see Table 6). Such large deviations from structurally predicted intensities have been observed even at liquid nitrogen temperatures, when the differences in rigidity were sufficient, for Fe^{III} complexes.[28]

At temperatures close to 5 K, an increase in line width and a slight asymmetry are observed. On further lowering temperature, magnetic dipolar splitting is partially established yielding a Zeeman spectrum at 4.2 K.

The Mössbauer spectrum of complex **8** consists of a simple symmetric doublet with parameters typical of low-spin iron(II) (Table 6). The spin-state of the iron in this complex remains unchanged up to 293 K, as evidenced by Mössbauer spectroscopy. The increase in isomer shift upon decreasing temperature is attributed to second-order Doppler effect.[26]

(26) Greenwood, N. N.; Gibbs, T. C. *Mössbauer Spectroscopy*; Chapman and Hall: New York, 1971; pp 9−11, 50−53.

(27) Londa, B.; Thalken, L.; Ceccarelli, C.; Glick, M.; Zhang, J. H.; Reiff, W. M. *Inorg. Chem.* **1983**, *22*, 1719.

(28) Thompson, K. L.; Zhao, L.; Xu, Z.; Miller, D. O.; Reiff, W. M. *Inorg. Chem.* **2003**, *42*, 128.

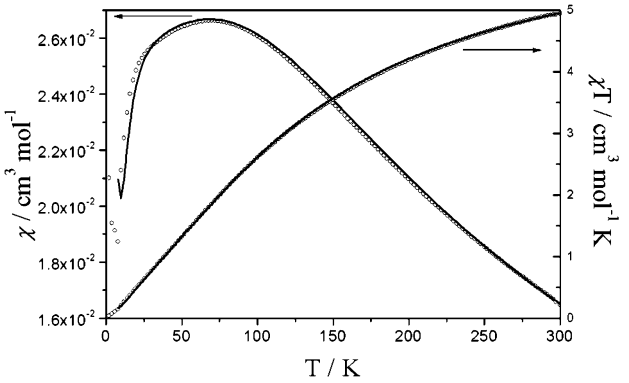

Figure 8. χ_M vs T and $\chi_M T$ vs T experimental data for complex **1**, and theoretical curves based on the Hamiltonian of eq 5.

Magnetic Properties. The thermal variation of the magnetic susceptibility χ_M has been measured for complexes **1**−**7**.

The thermal variations of χ_M and of the $\chi_M T$ product for complex **1** are plotted in Figure 8. The magnetic susceptibility increases from a value of 0.017 cm^3 mol^{-1} at 300 K to a broad maximum of 0.026 cm^3 mol^{-1} at ∼68 K, and then decreases at lower temperatures. The value of $\chi_M T$ is 4.96 cm^3 mol^{-1} K at 300 K, which is lower than the spin-only value for two noninteracting $S = 2$ metal centers (6.00 cm^3 mol^{-1} K). This value and the presence of a maximum in the χ_M versus T data are both indications of antiferromagnetic interactions. The slight increase of χ_M below 8 K is attributed to the presence of a small fraction of paramagnetic impurity (ρ). In order to fit these experimental data, a simple system of two exchange coupled iron(II) ions was considered. Attempts to fit without introducing any zero-field splitting terms yielded very poor results. Consequently, a zero-field splitting term D, common for both iron sites ($D_1 = D_2 = D$), was introduced, the implemented Hamiltonian being

$$\hat{H} = -2J\hat{S}_{Fe1}\hat{S}_{Fe2} + D(\hat{S}^2_{zFe1} + \hat{S}^2_{zFe2}) \qquad (5)$$

This model reproduced the experimental curve very well, except for a small disagreement at low temperature, which may be due to intermolecular interactions between adjacent dinuclear molecules through the weak Fe···S contacts yielding 1D chains (see Description of Structures subsection). The parameter values for the best fit (8−300 K range) were the following: $J = -13.7(5)$ cm^{-1}, $D = -1.8(3)$ cm^{-1}, $g = 2.10(1)$, $\rho = 0.7(2)$%, with a residual $R = 1.8 \times 10^{-4}$.

The $\chi_M T$ product for complex **2** is 5.44 cm^3 mol^{-1} K at 300 K and decreases rapidly with decreasing temperature indicating operation of antiferromagnetic interactions. Below ∼40 K, an increase in $\chi_M T$ is observed with a maximum of 2.56 cm^3 mol^{-1} K at ∼18 K, followed by a steep decrease down to 2 K. This behavior, which seems to indicate the presence of both antiferromagnetic and ferromagnetic interactions, has not been interpreted, due to the lack of structural information on complex **2**.

The thermal variation of the product $\chi_M T$ for complex **3**, under different fields, is plotted in Figure 9. Under a 10 kG field, the $\chi_M T$ product increases continuously from a value

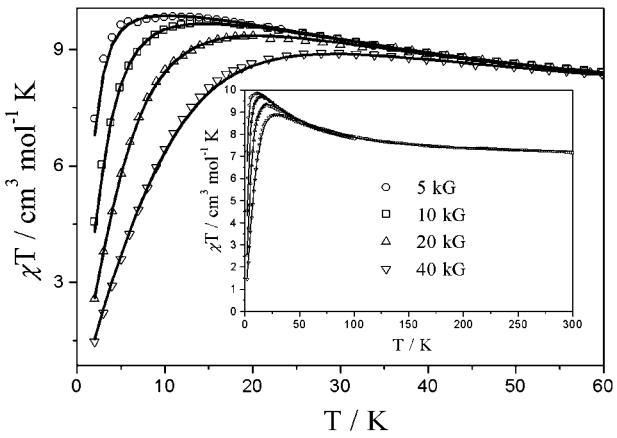

Figure 9. Low-temperature region of $\chi_M T$ vs T experimental data for complex **3**, and theoretical curves based on the Hamiltonian of eq 6, for several magnetic fields. The overall 2−300 K temperature range is shown in the inset.

of 7.17 cm^3 mol^{-1} K at 300 K, and reaches a maximum of 9.70 cm^3 mol^{-1} K at ∼15 K. This maximum is indicative of ferromagnetic interactions; increase of the applied field lowers the maximum and shifts it to higher temperatures, due to the additional splitting of the energy levels through Zeeman effect. The $\chi_M T$ decrease at low temperatures is associated with partial depopulation of the excited magnetic states, and zero-field splitting effects. A simple model of two interacting spins (isotropic interaction parameter J), employed as a first approach to simulate this behavior, yielded very poor results although the experimental curves for different magnetic fields were fitted simultaneously. Subsequent insertion in the model of a zero-field splitting (ZFS) term, common for both iron sites, improved the fits only slightly. It was then considered, on the grounds of structural and Mössbauer spectroscopy results, that the two iron sites are different enough for allowing consideration of different ZFS terms (D_1 and D_2 for Fe1 and Fe2, respectively). Implementation of this model brought about a remarkable improvement of the fits. The best fit parameters were the following: $J = 2.7$ cm^{-1}, $D_1 = 1.6$ cm^{-1}, $D_2 = -12.4$ cm^{-1}, $g = 2.140$, $\rho \approx 0$ with a residual $R = 6.9 \times 10^{-5}$ (solution A, not shown). In order to verify if this combination of D parameters was unique, we examined the error surface plot of the system (Figure S3). This confirmed the above solution, showing that there is no minimum for $D_1 = D_2$, and revealed a secondary minimum ($R = 3.3 \times 10^{-4}$). Thus, the necessity for different single ion axial terms was fully confirmed in agreement with the structural and Mössbauer data.

Additionally, in order to examine if a close $\pi-\pi$ stacking contact between complexes (see Description of Structures subsection) affected the magnetic properties of the compound, a model consisting of weakly interacting dinuclear molecules was examined. This model yielded essentially the same results as in solution A, with an additional intermolecular coupling constant of the order of 10^{-6} cm^{-1}. Therefore, it was concluded that no such interaction played a significant role in the bulk magnetic properties of complex **3**.

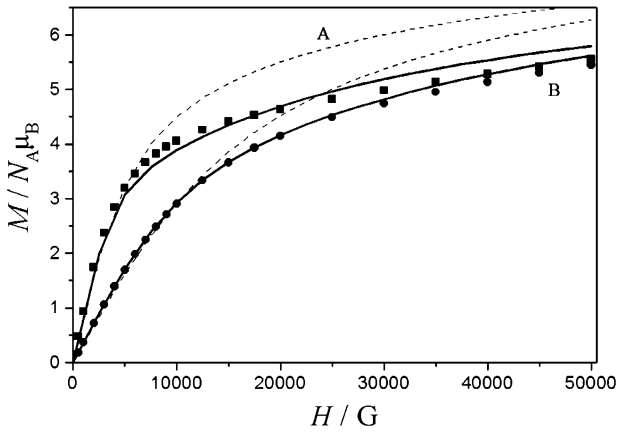

Figure 10. Variation of the magnetization M vs applied field H at 2 (■) and 5 (●) K for complex **3**. Dashed and solid lines correspond to the calculations based on solutions A and B, respectively.

The significant difference in rhombicity of the two iron sites intrigued us about the possibility to evaluate the local rhombic terms E_1 and E_2 for the Fe1 and Fe2 sites, respectively. The implemented spin Hamiltonian was

$$\hat{H} = -2J\hat{S}_{Fe1}\hat{S}_{Fe2} + D_1\hat{S}^2_{zFe1} + D_2\hat{S}^2_{zFe2} + E_1(\hat{S}^2_{xFe1} - \hat{S}^2_{yFe1}) + E_2(\hat{S}^2_{xFe2} - \hat{S}^2_{yFe2}) \quad (6)$$

This consideration brought about an improvement of the fit, with the following set of parameter values: $J = 3.0(3)$ cm^{-1}, $D_1 = 1.6(2)$ cm^{-1}, $E_1 = -0.35(6)$ cm^{-1} ($\lambda_1 = 0.22$), $D_2 = -12.2(7)$ cm^{-1}, $E_2 = 1.1(2)$ cm^{-1} ($\lambda_2 = 0.09$), $g = 2.14(1)$, $\rho \approx 0$, and a residual $R = 6.2 \times 10^{-5}$ (solution B, shown in Figure 9). In order to check if these additional E parameters have a true physical meaning and do not result in overparametrization, (i) we calculated and drawn the D_1 versus E_1 and D_2 versus E_2 surface error plots, and (ii) we carried out comparative theoretical calculations of the magnetization M versus H with the two sets of best χ_M versus T fit parameters (solutions A and B). The E_1 versus D_1 and E_2 versus D_2 plots (Figures S4 and S5, respectively) confirmed λ_1 as the sole E_1/D_1 minimum, and λ_2 as the absolute one among two minima. The M versus H theoretical calculations, carried out with the MAGPACK program package,[29] indicated that solution B is much closer to the experimentally observed behavior (Figure 10), thus confirming the significance of distinct E parameters for the Fe1 and Fe2 sites of complex **3**.

As a final comment, it should be mentioned that the D_2 value, although relatively high, is within the range of D values reported for iron(II) complexes,[2,30] and its negative sign is in line with the essentially tetragonal pyramidal character of the Fe2 ligand environment.

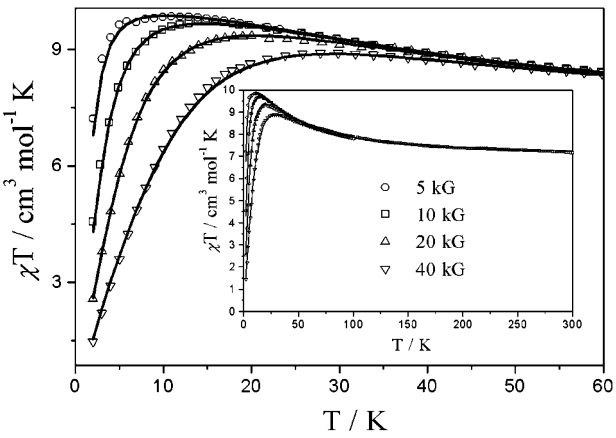

Figure 11. $\chi_M T$ vs T experimental data for complex **4** over the 2−50 K region under fields of 5, 10, 20, and 40 kG. The solid lines represent the best fits carried out simultaneously for all fields according to the Hamiltonian of eq 7. The behavior over the overall 2−300 K range under a field of 5 kG is shown in the inset.

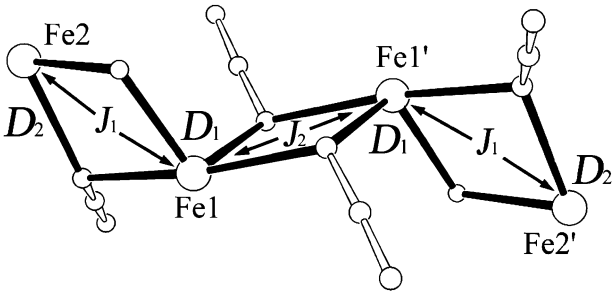

Figure 12. Spin-coupling scheme for complex **4**.

The thermal variation of the product $\chi_M T$ for the bis-dinuclear complex **4**, under different fields, is plotted in Figure 11. Under a 5 kG field, the $\chi_M T$ product rises slightly from a value of 14.52 cm^3 mol^{-1} K at 300 K, to reach a very broad maximum at ∼80 K. This increase and the fact that the maximum is field dependent indicate operation of ferromagnetic interactions. The rapid decrease at low temperatures is associated with partial depopulation of the excited magnetic states, and zero-field splitting effects. To account for this behavior, two types of magnetic interactions were assumed on structural grounds: an intradinuclear interaction, J_1, and an interdinuclear one, J_2. Attempts to fit the data taking into account only these isotropic interactions did not give satisfactory results. Similarly, when a common ZFS parameter was considered for all four iron(II) atoms, the fitting results were not satisfactory. Consequently, two ZFS parameters were considered, D_1 for the pentacoordinated external iron(II) sites and D_2 for the hexacoordinated internal ones (Figure 12). Equation 7 expresses the Hamiltonian describing this bis-dinuclear system:

$$\hat{H} = -2J_1(\hat{S}_{Fe1}\hat{S}_{Fe2} + \hat{S}_{Fe1'}\hat{S}_{Fe2'}) - 2J_2\hat{S}_{Fe1}\hat{S}_{Fe1'} + D_1(\hat{S}^2_{zFe2} + \hat{S}^2_{zFe2'}) + D_2(\hat{S}^2_{zFe1} + \hat{S}^2_{zFe1'}) \quad (7)$$

Due to the dependence of the susceptibility on the applied magnetic field, the data were simultaneously fitted for all magnetic field values. The best fit parameters were $J_1 = -0.7$ cm^{-1}, $J_2 = 2.9$ cm^{-1}, $D_1 = -1.3$ cm^{-1}, $D_2 = 20.3$ cm^{-1} with $g = 2.175$, $\rho \approx 0$ and a residual $R = 3.4 \times 10^{-4}$

(29) (a) Borrás-Almenar, J. J.; Clemente-Juan, J. M.; Coronado, E.; Tsukerblat, B. S. *Inorg. Chem.* **1999**, *38*, 6081. (b) Borrás-Almenar, J. J.; Clemente-Juan, J. M.; Coronado, E.; Tsukerblat, B. S. *J. Comput. Chem.* **2001**, *22*, 985.

(30) (a) Tommasi, L.; Shechter-Barloy, L.; Varech, D.; Battioni, J.-P.; Donnadieu, B.; Verelst, M.; Bousseksou, A.; Mansuy, D.; Tuchagues, J.-P. *Inorg. Chem.* **1995**, *34*, 1514. (b) Andres, H.; Bominaar, E. L.; Smith, J. M.; Eckert, N. A.; Holland, P. L.; Münck, E. *J. Am. Chem. Soc.* **2002**, *124*, 3012. (c) Sanakis, Y.; Power, P. P.; Stubna, A.; Münck, E. *Inorg. Chem.* **2002**, *41*, 2690.

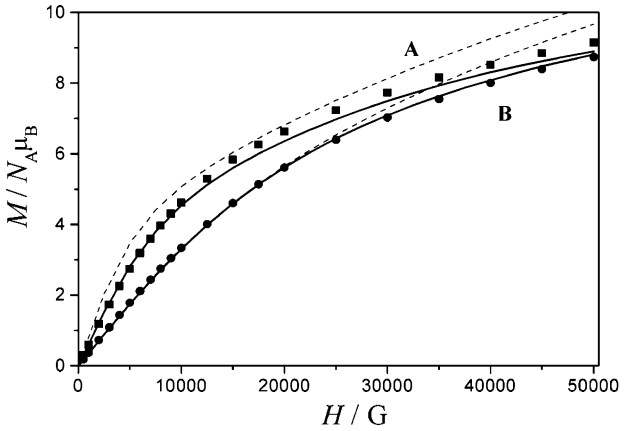

Figure 13. Variation of the magnetization M vs applied field H at 2 (■) and 5 (●) K for complex **4**. Dashed and solid lines correspond to the calculations based on solutions A and B, respectively.

(solution A, not shown). The high absolute value of D_2 and rather poor quality of the fit at low temperatures led us to examine the diagram of energy levels: despite the topology of the cluster which would require a $M_S = 0$ ground state, the lowest lying energy levels corresponding to solution A are the $M_S = \pm 4$ ones. In order to assess the validity of this fit, the magnetic data collected at all four fields in the 0−50 K range were simultaneously fitted, based on the model expressed in eq 7, and allowing for a paramagnetic impurity (ρ); the resulting parameter values were then used as initial values to fit the overall temperature range simultaneously for all fields. This resulted in a remarkable improvement of the fit at low temperatures. The derived parameters were the following: $J_1 = -0.09(5)$ cm^{-1}, $J_2 = 15.9(8)$ cm^{-1}, $D_1 = 5.7(4)$ cm^{-1}, $D_2 = 12.1(6)$ cm^{-1}, $\rho \approx 0$ with $g = 1.915(8)$ and a residual $R = 4.2 \times 10^{-5}$ (solution B, shown in Figure 11). The better agreement between the calculated and experimental data is reflected by the significant R decrease, the D_2 value is more reasonable than in solution A, and the lowest lying energy level in solution B is the $M_S = 0$ one (Figure S6).

In order to compare the quality and physical meaning of solutions A and B, we then carried out comparative theoretical calculations of the magnetization with the two sets of best χ_M versus T fit parameters (A and B). The M versus H theoretical calculations, carried out with the MAGPACK program package,[29] indicated that solution B is much closer to the experimentally observed behavior (Figure 13).

Finally, in order to assess the effect of the slight rhombicity structurally detected for sites Fe(2) and Fe(2′), a rhombic term E_2 was considered for these sites, yielding results qualitatively similar to solution B and a somewhat smaller residual R. The set of parameters derived from this fit was then used to calculate M versus H with the MAGPACK program package. This calculation, however, yielded poor results, and thus, this solution was discarded as unrealistic.

The zigzag arrangement of the four Fe^{II} atoms and the types of bridges in **4** being similar to those in $[Fe_2(pypentO)(NCO)_3]_2$ and $[Fe_2(pypentO)(N_3)_3]_2$ (pypentOH = 1,5-bis-[(2-pyridylmethyl)amino]pentane-3-ol),[2] it is worth comparing the structural parameters of the metal core for these first three examples of pseudohalido-bridged bis-dinuclear species in order to evaluate possible magneto-structural correlations. With regard to the intradinuclear interactions, this comparison may be extended to **3**.

The data gathered in Table 7 show that the intradinuclear Fe···Fe separations (3.14−3.20 Å for one alkoxo and one pseudohalido bridges) are very close to each other; the corresponding Fe−O−Fe angles span a narrow range, 103.2−106.7° while Fe−N−Fe and the Fe−N−Fe−O dihedral angle span larger ranges, 90.7−96.1° and 4.2−15°, respectively. There is no clear trend in the variation of any of these parameters which may be associated to the variation in intradinuclear magnetic interaction from 3 to −2.6 cm^{-1}. On the other hand, for the interdinuclear bridges (two pseudohalides) both the Fe···Fe separation (3.35 vs 3.46 and 3.50 Å) and Fe−N−Fe angle (100.1° vs 102.5−105.1°) are smaller in **4** where the interdinuclear ferromagnetic interaction is stronger (16 vs 0.7 and 0.75 cm^{-1}) compared to $[Fe_2(pypentO)(NCO)_3]_2$ and $[Fe_2(pypentO)(N_3)_3]_2$.[2]

The $\chi_M T$ versus T plot of complex **5** shows a continuous decrease from 4.81 cm^3 mol^{-1} K at 300 K, to 0.063 cm^3 mol^{-1} K at 2 K, indicative of antiferromagnetic interactions. The χ_M versus T plot, however, shows a continuous increase from 0.016 cm^3 mol^{-1} at 300 K to a maximum of 0.027 cm^3 mol^{-1} at ∼18 K, with a broad shoulder centered at ∼90 K. This behavior, which is rather difficult to model, might stem from weak intermolecular interactions within the solid. The intramolecular interaction should be responsible for the broad shoulder at ∼90 K, whereas a weaker interaction would cause the sharper maximum at 18 K. This type of interaction might be similar to the one observed in complex **1**, but the lack of detailed structural information does not allow us to attempt fitting these data.

The situation is similar for complex **6**: its $\chi_M T$ versus T product decreases continuously from 5.70 cm^3 mol^{-1} K at

Table 7. Compared Structural and Magnetic Parameters for Reported Pseudohalido-Bridged Ferrous Complexes

complex	Fe···Fe distance (Å)	Fe−O−Fe angle (deg)	Fe−N−Fe angle (deg)	Fe−N−Fe−O (Fe−N−Fe−N) dihedral angle (deg)	J (cm^{-1})
3 (this work)	3.17 (intra)	104.5	94.2	4.2	3
$[Fe_2(pypentO)(NCO)_3]_2$ (ref 2)	3.18 (intra)	103.9	92.4	12.9	0.6
	3.46 (inter)	106.7	102.5	0	0.7
4 (this work)	3.20 (intra)		93.4	5.6	−0.1
	3.35 (inter)	105.0	100.1	0	16
$[Fe_2(pypentO)(N_3)_3]_2$ (ref 2)	3.19 (intra)	103.2	96.1	11.4	-2.6_{av}
	3.14 (intra)		90.7	15	-2.6_{av}
	3.50 (inter)		103.5	6.6	0.75
			105.1		

300 K, to 0.091 $cm^3\ mol^{-1}$ K at 2 K, and the magnetic susceptibility increases continuously from 0.019 $cm^3\ mol^{-1}$ at 300 K to 0.047 $cm^3\ mol^{-1}$ at 2 K. In this case, however, the low-temperature maximum is concealed by the susceptibility increase due to a small fraction of paramagnetic impurity, and it appears as a shoulder.

Conclusions

The acpypentOH and acpybutOH dinucleating Schiff bases with N_4O donor sets possess the ability of imposing, in combination with pseudohalides, various coordination environments to iron(II), endowing the resulting ferrous complexes with unexpected and original physical properties.

$[Fe_2(acpypentO)(O_2CMe)(NCS)_2]$ (**1**) and $[Fe_2(acpypentO)(O_2CMe)(NCSe)_2]$ (**2**) are dinuclear species in which the inequivalent HS Fe^{II} sites are bridged by the alkoxo oxygen atom of the symmetrical acpypentO$^-$ Schiff base and one acetato anion. The slight structural differences in ligand environment between the two ferrous centers are significant enough to be sensed by Mössbauer spectroscopy which shows two HS Fe^{II} quadrupole split doublets. The intradinuclear magnetic interaction mediated by the alkoxo and acetato bridges of **1** is antiferromagnetic ($J \sim -14\ cm^{-1}$) and the iron(II) anisotropy is weak ($D \sim -2\ cm^{-1}$).

$[Fe_2(acpypentO)(NCO)_3]$ (**3**) is a dinuclear species in which the inequivalent HS Fe^{II} sites are bridged by the alkoxo oxygen atom of the symmetrical acpypentO$^-$ Schiff base and one end-on NCO anion. The significant structural differences in geometry of the ligand environment between the two ferrous centers are reflected by the presence of two very different HS Fe^{II} quadrupole split doublets. The intradinuclear magnetic interaction mediated by the alkoxo and cyanato bridges of **3** is ferromagnetic ($J = 3\ cm^{-1}$), and the differences in symmetry of the Fe^{II} ligand environments are reflected by significant differences in the anisotropy parameters of Fe1 and Fe2 ($D_1 = 1.6\ cm^{-1}$, $E_1 = -0.35\ cm^{-1}$ ($\lambda_1 = 0.22$), $D_2 = -12.2\ cm^{-1}$, $E_2 = 1.1\ cm^{-1}$ ($\lambda_2 = 0.09$). Compound **3** is the second $Fe^{II}-NCO-Fe^{II}$ bridged complex ever described: its ferromagnetic behavior, similar to that of $[Fe_2(pypentO)(NCO)_3]_2$ (pypentOH = 1,5-bis[(2-pyridylmethyl)amino]pentane-3-ol),[2] suggests that end-on NCO is an as good as, or even better, ferromagnetic coupler for Fe^{II} than N_3^-.

$[Fe_4(acpypentO)_2(N_3)_6]$ (**4**) is a bis-dinuclear species in which the inequivalent HS Fe^{II} sites are bridged by the alkoxo oxygen atom of the symmetrical acpypentO$^-$ Schiff base and one end-on N_3^- anion, and the symmetry related Fe^{II} sites are bridged by two end-on N_3^- anions. The differences in ligand environment between the two types of ferrous centers (N_5O, octahedral for Fe1(1′) and N_4O, pyramidal for Fe2(2′)) are reflected by the presence of two very different HS Fe^{II} quadrupole split doublets. The intradinuclear magnetic interactions mediated by the alkoxo and azido bridges of **4** are weakly antiferromagnetic ($J_1 \sim -0.1\ cm^{-1}$) while the interdinuclear interaction mediated by the two azido bridges is ferromagnetic ($J_2 \sim 16\ cm^{-1}$); the differences in ligand environment between the two types of Fe^{II} centers (octahedral Fe1(1′) and pyramidal Fe2(2′)) are reflected by significant differences in the anisotropy parameter ($D_1 = 5.7\ cm^{-1}$, $D_2 = 12.1\ cm^{-1}$). Compound **4** is the second $Fe^{II}-N_3-Fe^{II}$ bridged complex ever described: its magnetic behavior is qualitatively similar to that of $[Fe_2(pypentO)(N_3)_3]_2$: the intradinuclear magnetic interactions (alkoxo and azido bridges) are weakly antiferromagnetic while the interdinuclear interaction (two azido bridges) is ferromagnetic in both compounds;[2] the differences in ligand environment between the octahedral and pyramidal Fe^{II} centers are reflected by similar differences in the anisotropy parameter of both compounds.[2]

$[Fe_2(acpybutO)(O_2CMe)(NCS)_2]$ (**5**), $[Fe_2(acpybutO)(O_2CMe)(NCO)_2]$ (**6**), and $[Fe_2(acpybutO)(O_2CMe)(N_3)_2]$ (**7**) are dinuclear species in which the inequivalent HS Fe^{II} sites are bridged by the alkoxo oxygen atom of the asymmetrical acpybutO$^-$ Schiff base and one acetato anion. The differences in ligand environment between the two ferrous centers are reflected by the presence of two different HS Fe^{II} quadrupole split doublets. In the absence of X-ray crystal structure, the magnetic data of complexes **5**−**7** were not fitted; qualitatively, however, it may be stated that the intradinuclear magnetic interaction mediated by the alkoxo and acetato bridges is antiferromagnetic as in the similarly bridged complexes **1** and **2**.

$[Fe(acpybutOH)(NCS)_2]$ (**8**) is a mononuclear species in which the octahedral LS Fe^{II} site is in an N_6 environment provided by the four N atoms of the protonated asymmetrical acpybutOH Schiff base and two thiocyanato anions.

The antiferromagnetic behavior of complexes **1**, **2**, and **5**−**7** is in line with that of previously reported dinuclear complexes including one alkoxo and one carboxylato bridges between transition metals.[3b,31] The magnetic behavior of complexes **3** and **4** is in line with that[2] of $[Fe_2(pypentO)(NCO)_3]_2$ and $[Fe_2(pypentO)(N_3)_3]_2$, and together, they yield the first pieces of information on the magnetic interactions mediated by end-on bridging pseudohalides between Fe^{II} centers: (i) The magnetic interactions mediated by one alkoxo and one end-on cyanato bridges are weak, and end-on NCO seems to be a better ferromagnetic coupler for Fe^{II} than N_3^-. The range of values for the ferromagnetic interactions mediated by two end-on bridging cyanato or two end-on bridging azido is larger, and the trend seems to be reversed. However, additional data are needed before we may draw reliable conclusions from a comparison of the magnetic interactions mediated by end-on NCO and N_3^- bridges between Fe^{II} centers.

Acknowledgment. A.K.B. and J.-M.C.-J. thank the European Community for support through doctoral and postdoctoral grants within the framework of the TMR contract FMRX-CT980174.

Supporting Information Available: Additional figures, additional table, and crystallographic data in CIF format. This material is available free of charge via the Internet at http://pubs.acs.org.

IC0351904

(31) (a) Mazurek, M.; Bond, A. M.; O'Connor, M. J.; Wedd, A. G. *Inorg. Chem.* **1986**, *25*, 906. (b) Nishida, Y.; Kida, S. *J. Chem. Soc., Dalton Trans.* **1986**, 2633.